Cretaceous Research 85 (2018) 214–231

Contents lists available at ScienceDirect

Cretaceous Research

journal homepage: www.elsevier.com/locate/CretRes

A juvenile *Tuarangisaurus keyesi* Wiffen and Moisley 1986 (Plesiosauria, Elasmosauridae) from the Upper Cretaceous of New Zealand, with remarks on its skull ontogeny

Rodrigo A. Otero [a, *], José P. O'Gorman [b, c], William L. Moisley [d], Marianna Terezow [e], Joseph A.W. McKee [f]

[a] Laboratorio de Ontogenia y Filogenia, Departamento de Biología, Facultad de Ciencias, Universidad de Chile, Las Palmeras, 3425, Santiago, Chile
[b] División Paleontología Vertebrados, Museo de La Plata, Universidad Nacional de La Plata, Paseo del Bosque s/n., B1900FWA, La Plata, Argentina
[c] CONICET: Consejo Nacional de Investigaciones Científicas y Técnicas, Argentina
[d] 141 Puriri Street, Castlecliff, Whanganui, 4501, New Zealand
[e] GNS Science, 1 Fairway Drive, Avalon, P.O. Box 30368, Lower Hutt, 5040, New Zealand
[f] P.O. Box 5085, Terrace End, Palmerston North, 4441, New Zealand

ARTICLE INFO

Article history:
Received 28 April 2017
Received in revised form
23 August 2017
Accepted in revised form 12 September 2017
Available online 18 September 2017

Keywords:
Austral elasmosaurids
Ontogeny
Juvenile
Weddellian Province
Late Cretaceous

ABSTRACT

This paper presents the detailed description of a remarkable skull and partial postcranial skeleton of a very juvenile elasmosaurid referred to *Tuarangisaurus keyesi* (CD 427), from the upper Campanian-lower Maastrichtian levels of the Tahora Formation, New Zealand. The following points are discussed: i) the conspecific status of CD 427 with *T. keyesi*, ii) clarification of several cranial sutures in the adult holotype of *T. keyesi* by comparison with the clearly open sutures in the juvenile specimen; iii) morphologic changes undergone by the skull during the ontogeny of *T. keyesi*; iv) a first look at the postcranial skeleton of *T. keyesi*. The studied specimen holds a great significance because it represents one of the rarely-available juvenile elasmosaurid skulls known worldwide. As a result, we provide the first insights regarding the skull ontogeny of an austral elasmosaurid plesiosaurian.

1. Introduction

Tuarangisaurus keyesi Wiffen and Moisley 1986 is a taxonomic concept fixed to a fairly complete skull, atlas-axis and anterior cervical vertebrae, recovered from the Mangahouanga Stream, a northern tributary of Te Hoe River, inland Hawke's Bay, New Zealand (Fig. 1). The holotype comes from the Maungataniwha Sandstone Member of the Tahora Formation. Because the material was recovered from transported boulders, its chronostratigraphic provenance cannot be refined beyond the upper Campanian-lower Maastrichtian (Vajda and Raine, 2010). Along with the original description, Wiffen and Moisley (1986) illustrated few fragmentary specimens from Mangahouanga Stream. Among them, CD 427 represents a remarkable juvenile specimen, preserving both cranial and postcranial elements. The presence of skull material in CD 427 is particularly important as *T. keyesi* is the only non-aristonectine elasmosaurid from the Weddellian Province with well-known skull anatomy; in addition, CM Zfr 115 preserves few cranial elements. The other two Weddellian, non-aristonectine elasmosaurid taxa, *Vegasaurus molyi* and *Kawanectes lafquenianum* are based only on postcranial material (O'Gorman et al., 2015; O'Gorman, 2016). Here we review this particular specimen, with special focus on the skull anatomy. The latter indeed preserves more elements than those first described by Wiffen and Moisley (1986) allowing a direct comparison with the *T. keyesi* holotype skull. Several skull elements in the juvenile are similar to those preserved in the *T. keyesi* holotype (adult specimen). Osteological differences observed in the juvenile can be explained by ontogenetic changes that also occur in extant reptiles.

Specimen CD 427 provides a remarkable opportunity for studying the elasmosaurid skull ontogeny within a single species,

* Corresponding author.
E-mail addresses: otero2112@gmail.com (R.A. Otero), joseogorman@fcnym.unlp.edu.ar (J.P. O'Gorman), hawkesbaypalaeogroup@gmail.com (W.L. Moisley), m.terezow@gns.cri.nz (M. Terezow), joseph_mckee@hotmail.com (J.A.W. McKee).

http://dx.doi.org/10.1016/j.cretres.2017.09.007
0195-6671/

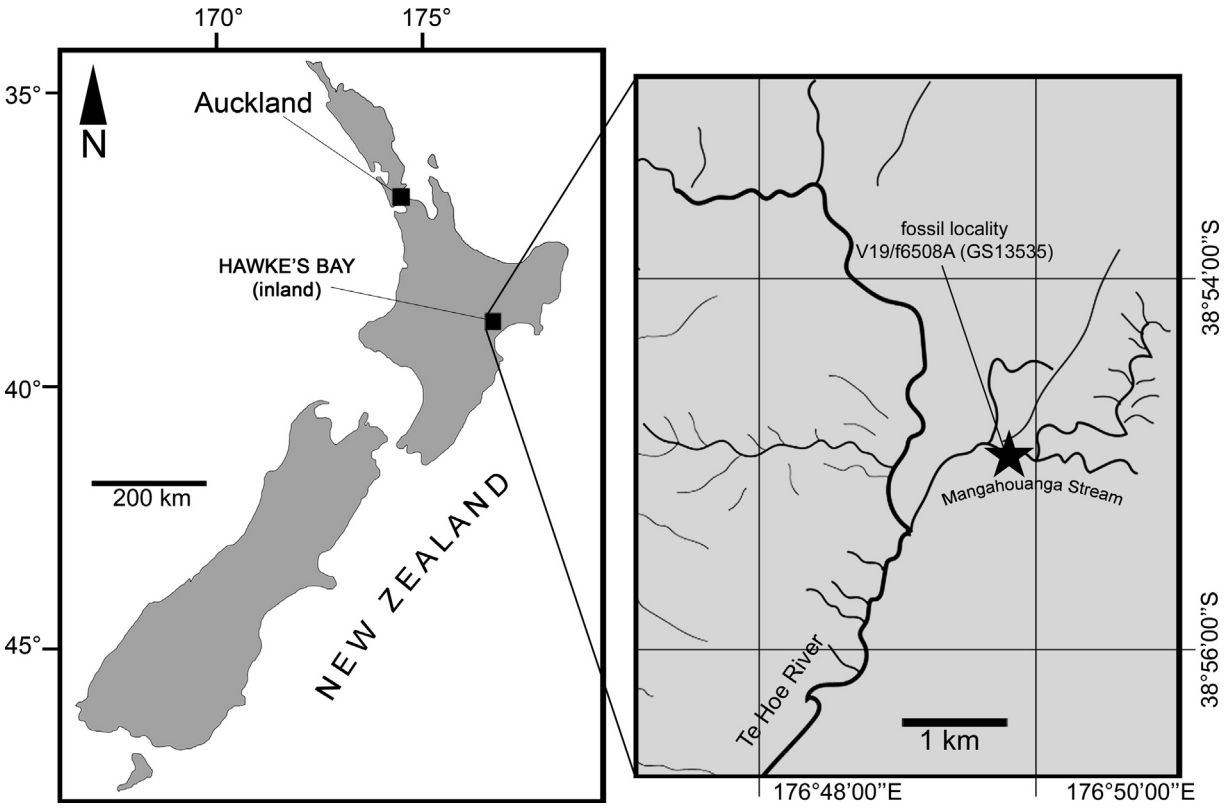

Fig. 1. Map indicating the Mangahouanga Stream, east of Te Hoe River, inland Hawke's Bay, in the North Island of New Zealand. The studied specimen (CD 427) comes from the fossil locality V19/f6508A (collected by Joan Wiffen and William Moisley in 1976) indicated with the star.

being the first skull ontogenetic series available for a Late Cretaceous taxon from the southern hemisphere. Furthermore, the material preserves several postcranial elements that allow us a better understanding of the trunk and anterior extremities of *T. keyesi*, previously unknown in its holotype.

2. Locality and geologic setting

'Bill's Baby', the nickname given to the very juvenile specimen CD 427 found by William L. Moisley, was collected from the locality V19/f6508A (GS1535) NZMS 260 Map Sheet V19, Grid Reference 419 470, as pointed out by Wiffen and Moisley (1986). This is placed in the course of the Mangahouanga Stream, 200 m upstream from the forestry road bridge, inland Hawke's Bay, North Island, New Zealand (Fig. 1, Fossil Record Electronic number V19/f6508A, GS 13535). Rocks cropping out in this locality are part of the Maungataniwha Sandstone Member of the Tahora Formation. This represents the basal unit of Late Cretaceous age in northeastern New Zealand (Isaac et al., 1991; Cutten, 1994). The Maungataniwha Sandstone Member is a ca. 400 m thick unit mostly comprised of poorly bedded sandstones. Its depositional environment has been interpreted as a fully marine, near-shore, shallow water setting with moderate to high energy, possibly within an estuary, bay, or inlet. Deposition occurred during several minor transgressive – regressive cycles (Crampton and Moore, 1990). Fossil assemblages include marine invertebrates and tracefossils (Glaessner, 1980; Crampton, 1990; Crampton and Moore, 1990; Feldmann, 1993; Eagle, 1994), indicating at least three different habitats. Vertebrates found in the unit include chondrichthyans and osteichthyans (Keyes, 1977; Wiffen, 1983) plesiosaurs, mosasaurs, turtles (Wiffen, 1980, 1981, 1990a,b; Wiffen and Moisley, 1986), as well as continental vertebrates represented by fragmentary remains of dinosaurs and pterosaurs (Wiffen and Molnar, 1988; Wiffen and McKee, 1990; McKee and Wiffen, 1998). The terrestrially-derived fauna suggests the presence of a nearby river mouth or delta (Crampton and Moore, 1990).

In the lower Mangahouanga Stream (Fig. 1), the age of the Maungataniwha Sandstone Member has been assigned to the upper Piripauan-lower Haumurian New Zealand stages, equivalent to the Campanian-Maastrichtian (Warren and Speden, 1978). Microfossils and palynomorphs suggested that the lower 100 m could be refined to the Piripauan, and the upper 200–250 m to the Haumurian (Crampton and Moore, 1990). Most marine reptile remains from the unit have been recovered from the calcareous and phosphatic concretions in the float of the river bed. Dinocyst assemblages indicate that the concretions may derive from at least two horizons (Young and Hannah, 2010), while plesiosaur-bearing concretions indicate different stages between the lower to upper Haumurian (lower Campanian to lower Maastrichtian). Based on the assemblage of pollen taxa, dinocysts and megaspores, Vadja and Raine (2010) proposed an upper Campanian-lower Maastrichtian age for the plesiosaur-bearing boulders.

3. Material and methods

The material examined is part of the National Paleontological Collection (NPC) held at GNS Science, Lower Hutt, New Zealand. CD 425 and CD 426 (holotype of *Tuarangisaurus keyesi*) and CD 427 ('Bill's Baby') are part of a collection of 31 partial elasmosaur specimens, recovered by W.L. Moisley, T. Crabtree, M.A. Wiffen and J. Wiffen, over 10 years of summer fieldwork in the Mangahouanga Stream, before 1986 (Wiffen and Moisley, 1986). According to these authors, each specimen was reduced on site by mechanic means, using cutting saw, hammers and chisels for facilitating their transport within

backpacks, due to the remoteness of the area. Particularly, CD 427 (skull and postcranial skeleton) was found within a single concretion which was split in two parts for easier transport. Further preparation considered mechanical reduction and final detail was obtained by acetic acid extraction performed by J. Wiffen, W.L. Moisley and T. Crabtree (Wiffen and Moisley, 1986). The juvenile specimen CD 427 was compared with CD 425 and CD 426, holotype of *Tuarangisaurus keyesi*. Data collection of the latter was done during April and May 2013, at Museum of New Zealand Te Papa Tongarewa, Wellington, New Zealand. Data collection of CD 427 was carried out during the same time at GNS Science, Lower Hutt, New Zealand.

The skull and postcranial skeleton of CD 427 were digitally reconstructed in a composite picture in order to illustrate their general anatomy and for comparisons of its relative size with *T. keyesi* holotype (Fig. 2).

Institutional Abbreviations—**AMNH**, American Museum of Natural History, New York, USA; **CD**, Chordata collection, National Paleontological Collection, GNS Science, Lower Hutt, New Zealand; **MML PV**, Museo Municipal de Lamarque, Rio Negro Province, Argentina; **SGO.PV.**, Área Paleontología, Museo Nacional de Historia Natural, Santiago, Chile.

4. Systematic paleontology

Sauropterygia Owen, 1860
Plesiosauria de Blainville, 1835
Xenopsaria Benson and Druckenmiller, 2014
Elasmosauridae Cope, 1869
Tuarangisaurus Wiffen and Moisley, 1986

Tuarangisaurus keyesi Wiffen and Moisley, 1986

Holotype. CD 425 and CD 426. *Tuarangisaurus keyesi* Wiffen and Moisley 1986, monotypic. A skull, atlas-axis and anterior cervical vertebrae.
Locality and horizon. Mangahouanga Stream, inland Hawke's Bay, New Zealand. Fossil Record File locality number V19/f6909 (GS11359). Tahora Formation, Maungataniwha Sandstone Member, late Campanian-early Maastrichtian (Vajda and Raine, 2010).
Diagnosis. T. keyesi shows one autapomorphy: ectopterygoid with large boss on the ventral surface, having a posteriorly directed long process (O'Gorman et al., 2017). The following combination of characters has been considered unique to *T. keyesi* (Wiffen and Moisley, 1986; O'Gorman et al., 2017): premaxillae fused and forming a convex surface between naris, without medial ridge; premaxillae extended posteriorly and having a folded, rugose surface between orbits; frontals separated by premaxillae; five teeth in each premaxilla, differing from *Eromangasaurus australis* (three lateral pairs, one midline) and all aristonectines (seven or more); small diastema-like space between premaxillary and maxillary teeth; fifteen maxillary alveoli, differing from all aristonectines (38 or more); ventral margin of the orbit convex and formed mostly by the maxilla, differing from *E. australis* and *Futabasaurus suzukii*; no parietal foramen, differing from *Callawayasaurus*; anterior ramus of pterygoids overlaps posterior half of vomer; mandibular symphysis short, extending back as far as the fourth alveolus (Contra O'Gorman et al., 2017). 20–21 dentary alveoli; high coronoid process, differing from *Libonectes morgani* and *Zarafasaura oceanis*; atlas rib as long as the axis rib and dorsoventrally compressed axis rib differing from *Vegasaurus molyi*; axis neural spine does not project posterior to the postzygapophysis, differing from *Thalassomedon haningtoni.*

Tuarangisaurus keyesi Wiffen and Moisley, 1986
Figs. 2–10
cf. *Tuarangisaurus keyesi*: In Wiffen and Moisley (1986).
Aristonectinae indet.: In Araújo et al. (2015).

Referred specimen studied here. CD 427. A partial disarticulated skull, several axial elements, ribs, gastralia, girdle fragments and an articulated limb of a single, juvenile individual.
Locality, horizon and age. Mangahouanga Stream, Te Hoe River, inland Hawke's Bay, New Zealand. Fossil Record File locality number V19/f6508A (GS13535). Maungataniwha Sandstone Member of the Tahora Formation, upper Campanian-lower Maastrichtian.

5. Description of CD 427

General Remarks—CD 427 preserves postcranial elements, however, these do not overlap with the sparse postcranial elements of the holotype of *T. keyesi* (CD 425 and 426), consisting in few cervical vertebrae. Thus, comparisons and ontogenetic observations are here restricted exclusively to the skull elements. However, a description of the postcranial elements is also provided.

Ontogenetic Stage—Most of the skull elements are non-fused. This and the small size of the specimen unequivocally support the inferred juvenile condition. The same condition is noted in the articulated limb where all the articular surfaces between the different elements appear as rounded and undifferentiated surfaces, typical of very juvenile individuals (Brown, 1981). Also, dorsal vertebrae show visible neurocentral sutures. A single dorsal vertebra visible in articular view in a separate block with gastroliths, allows us to observe the neural arch separated from the centrum. Considering the presence of very delicate elements already ossified, the full contact between several skull elements, and the evident presence of gastroliths, the specimen is considered a postnatal individual of very early ontogenetic age.

Premaxillae—Only the posterior midline extension of the fused premaxillae is preserved attached in anatomical position between the frontals. In dorsal view, its posteriormost part ends in an extended, interdigitated suture which is still open and filled with sandstone matrix. A similar suture line is present in the anterior midline extension of the parietals, indicating that the parietals and the premaxilla should contact in the adult through a complex suture. In ventral view, the midline posterior extension of the premaxilla is medially covered by the frontals.

Maxillae—Both maxillaries are preserved and they are fairly complete (Fig 3A–D). The left maxilla is articulated with the left postorbital + postfrontal as well as the left jugal. Together, these are attached, overlying the bony elements that form the orbital part of the skull roof (Fig. 3A, B). The right maxilla is isolated. Both maxillaries have very good three-dimensional preservation; they are not crushed or deformed. Both maxillaries show a lateromedial, bowl-like lateral extension (see Figs. 2A, 7A) coincident with the middle part of the orbital ventral margin. Anterior to this lateral extension of the orbit, the labial surface of each maxilla bears abundant foramina. They are also present under the orbital margin; however, in this zone the foramina are less abundant. Laterally, both maxillaries possess a rostrally-oriented dorsal process in their anterior parts; these processes form an angle of ca 60° to the horizontal. This dorsal process forms the anterior margin of the orbit, and together with the anterior part of the maxilla, it also forms the posterior and ventral margins of the external naris. The dorsal tips of both dorsal processes are complete and they are slightly expanded, having a rugose distal end, likely for cartilaginous attachment. In lateral view, the ventral margin of the orbit is slightly convex (Fig. 3C, D), overhanging to the tooth outline (the same occurs in the holotype of *T. keyesi*). The contact with the postorbital + postfrontal is clear and it has an interdigitated suture line. The posterior part of the maxilla tapers ventrally to the jugal.

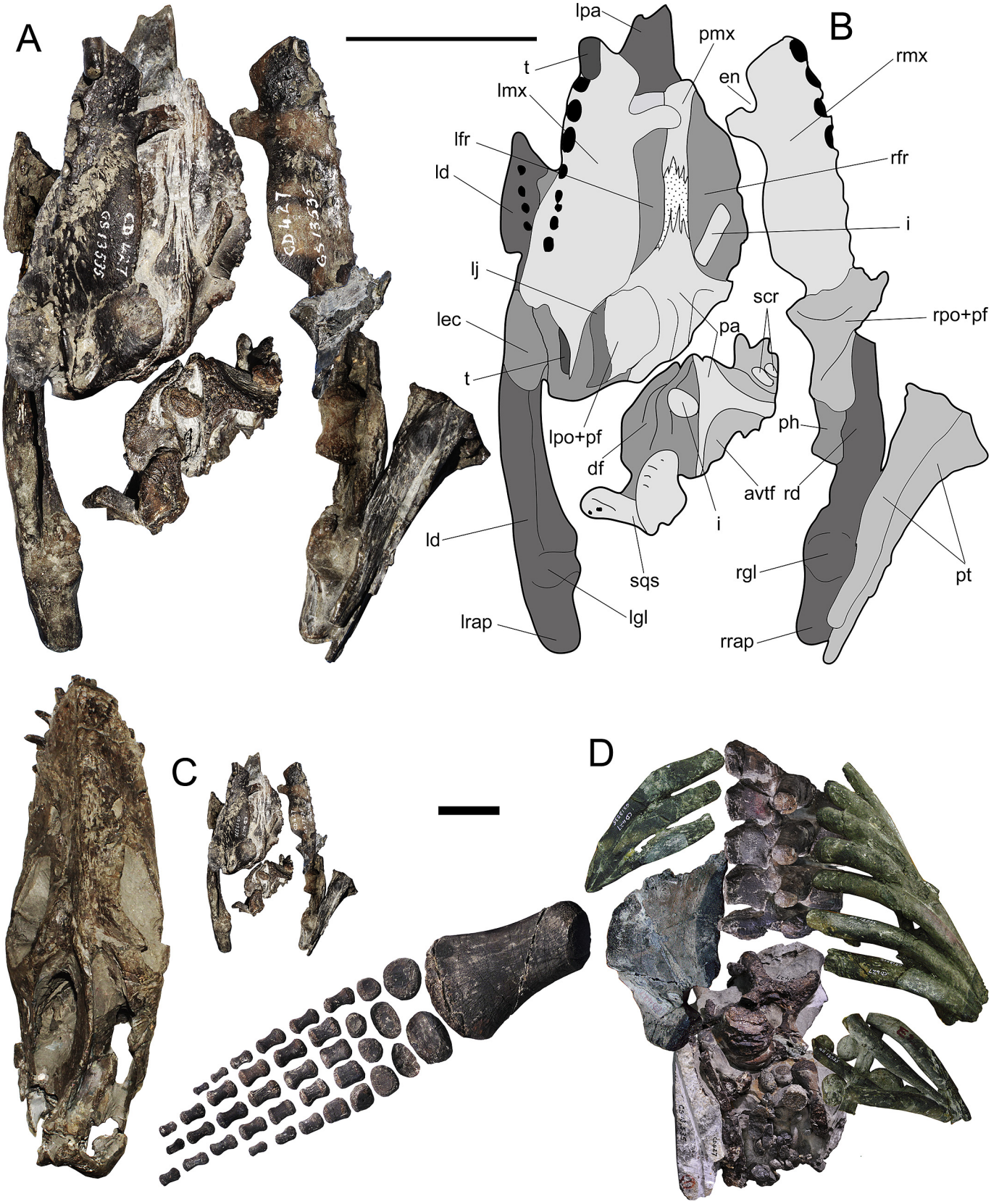

Fig. 2. CD 427. **A**. *Tuarangisaurus keyesi*, referred. Composite picture of the different skull elements in dorsal view. **B**. Schematic of the skull. CD 425, holotype of *Tuarangisaurus keyesi*. **C**. CD 425 and CD 427. **D**. Composite of the postcranial elements in dorsal view. Anatomical abbreviations: **avtf**, anteroventral margin of the temporal fossa; **df**, dentary fragments; **en**, external naris; **i**, indeterminate;**ld**, left dentary; **lec**, left ectopterygoid; **lfr**, left frontal; **lgl**, left glenoid; **lj**, left jugal;**lmx**, left maxillary; **lpa**, left palatine; **lpo**+**pf**, left postorbital + postfrontal; **lrap**, left retroarticular process; **pa**, parietals; **pmx**, premxillary; **ph**, phalanx; **pt**, pterygoids; **rd**, right dentary; **rfr**, right frontal; **rgl**, right glenoid; **rmx**, right maxillary; **rpo**+**pf**, right postorbital + postfrontal; **rrap**, right retroarticular process; **scr**, sclerotic ring; **sqs**, squamosal socket for the quadrate; **t**, tooth. **A**, **B**, Scale bar equals 50 mm. **C**, **D**, scale bar equals 10 mm.

The occlusal part of the left maxilla preserves 14 alveoli. The anteriormost alveolus is covered by a loose tooth; from the seventh alveoli and backwards, teeth are in anatomical position, however, their crowns are broken. An isolated posterior tooth remains next to the last posterior alveolus and over the labial surface. The right maxilla only retains its first anterior tooth in anatomical position, while all the other maxilla alveoli are empty. This element preserves thirteen alveoli and the anterior margin of the last fourteenth alveolus. In both maxillaries, the alveoli are occlusally oriented (Fig. 3D). Also, in both maxillae the six anterior alveoli are comparatively larger than the others, while the largest alveolus is the third anterior, positioned just anterior to the lateral expansion of the orbit (Fig. 3D). The right maxilla allows us to observe several resorption pits situated in the lingual margin of the alveolar row. The high number of these and their proximity between each pit give them a groove-like aspect, being delimited by a lingual ridge. It is difficult to individualize the number of resorption pits present on the right maxilla, while in the left one, these are obscured by the siltstone matrix. Ventrally, both maxillaries show a bowed, laterally convex alveolar row.

Jugals—This element is a slender, axially-oriented bone that occurs between the posterior process of the maxilla and below the postorbital + postfrontal (Fig. 3A, B).

Postorbital+postfrontals—The two postorbital + postfrontals are preserved. The left one (Fig. 3A, E) is attached to the maxilla in anatomical position and is posteriorly broken. A tenuous suture line with the left jugal is visible, allowing us to separate the postorbital + postfrontal from the former (Fig. 3E). However, the contact between postorbital and postfrontal is not visible even in the very juvenile stage of the specimen. The right postorbital + postfrontal (Fig. 3F) is isolated, anteriorly incomplete, and it preserves most of its posterior extension. A small posterior fragment of the right jugal is also attached to this portion. This complex has a small dorsal process (rising from the postfrontal), which is involved in the closure of the posterior margin of the orbit later in the ontogeny of the animal. The right postorbital + postfrontal allows us to observe an anterior concavity consistent with the posteroventral surface of the eye ball. Its posterior extension shows a dorsal, grooved surface, consistent with the contact with the anterior extension of the squamosal.

Frontals—Both frontals are almost completely preserved (Fig. 4A–D). Dorsally, the medial contact between them is obscured by the posterior midline extension of the premaxilla and by the anterior midline extension of the parietals. However, in ventral view, both frontals meet in the midline. Such contact indeed occurs in the adult holotype, being detected through CT-Scan (O'Gorman et al., 2017). Ventrally, the frontals form a duct here interpreted as the olfactory duct. Anteriorly, in each side of the olfactory duct there are two, well-excavated concavities separated from the olfactory duct by a medial septum. Instead, laterally, each concavity is separated from the orbit by a shallow septum. In addition, both frontals have a more concave ventral surface, which is consistent with the placement of the eye ball. In ventral view, the left frontal (the better preserved) preserves the dorsal margin of the orbit.

Parietals—The anterior parts of both parietals are preserved in anatomical position, attached to the frontals (Fig. 4A–D). Dorsally, the anterior midline extension of the parietals shows a very interdigitated suture line that is barely separated from the mid posterior extension of the premaxilla. Likely, both elements would connect in late ontogenetic stages, judging by the very similar type of suture and by the proximity between both elements. The posterodorsal preserved portion shows an incipient sagittal crest. Even in the early ontogenetic stage of the specimen, there is no evidence of a pineal foramen (Fig. 4A, B). In ventral view, the parietals have a triangular anterior extension that contacts the frontals through a straight suture line. An additional part of the right parietal is preserved in a separate block containing multiple crushed elements (Fig. 5A, B).

Squamosals—Only the posteroventral part of one squamosal is preserved, attached to other crushed elements (Fig. 5A–D). Its laterality is difficult to determine because of its deformation. It has a rounded, rugose end interpreted as the bone layer that covers the quadrate. The preserved portion indeed resembles the socket that covers the quadrate; however, its preservation and ontogenetic stage make further anatomical interpretations difficult.

Ectopterygoids—Both ectopterygoids are preserved. The right ectopterygoid is attached to other crushed elements (Fig. 5A–D). The left one is attached ventroposteriorly to the left postorbital + postfrontal, being crushed and slightly twisted from its anatomical position (Fig. 5E). It is only visible in ventrolateral view. Its ventral part is flattened. A posteroventral process rises from its posteromedial margin. This is bent due to taphonomic conditions.

Palatine—A good part of the anterior left palatine is preserved as an isolated element (Fig. 5F). Dorsally, this has a triangular outline with a straight medial contact for the pterygoid. Its posterior part has a concavity consistent with the internal ventral margin of the orbit. A small, squared indeterminate bone remains attached to the orbital bowl. The posterior end of the right palatine is also preserved, attached to the posterior part of the right mandibular ramus (Fig. 6A–D).

Pterygoids—Both pterygoids are preserved, but they lack their posterior ends. These are disarticulated and placed together with the right palatine, all attached to the posterior right mandibular ramus (Fig. 6A, B). They are axially elongated and dorsoventrally thin. The right pterygoid (Fig. 6C, D) preserves its articular facet for the basioccipital. In posterior view, both pterygoids are triradiate, with two projections forming the basioccipital facet and the remaining projection extending laterally and forming most of the bone.

Mandibular rami—Both incomplete rami are preserved, lacking the mandibular symphysis. In dorsal view, the left posterior ramus shows a short retroarticular process, a shallow, poorly differentiated glenoid cavity, and a dorsolabial projection of the surangular (Fig. 7A). In lingual view (Fig. 7B), the same element clearly shows the suture contact between the articular and the surangular. The retroarticular process is indeed formed by a similar participation of the surangular, dorsally, and the angular, ventrally. Anterior to the glenoid, the surangular has a diagonal suture with the articular. The left angular is fairly complete. Its anterior end is attached to the posterior part of the left dentary. The respective coronoid is lost. The right mandibular ramus (Fig. 7C, D) shows similar features, however, it remains partially obscured by the pterygoids and one phalanx. The left surangular can be observed in cross-section (Fig. 7E), just before the following portion with part of the dentary attached. The anteriormost preserved fragment of the left ramus (Fig. 7F) shows the labial wall of the dentary as well as a dorsal concavity consistent with an alveolus. The lingual face of the same material shows the separate surangular, dorsally displaced, leaving the Meckellian canal visible in lingual view.

Dentition—Two isolated teeth are associated with CD 427 (Fig. 7G, H). Both have a crown between 10 and 15 mm, with their labial face slightly convex. Their visible labial surfaces are profusely cracked due to taphonomic conditions. There are slight striations (as soft ridges) in the base of each crown. Both teeth have lingual surfaces with striated enamel. One tooth has a root that represents nearly one-third of the complete tooth height. The second tooth has a root nearly half of the entire tooth height. Their small size is consistent with the juvenile stage of CD 427.

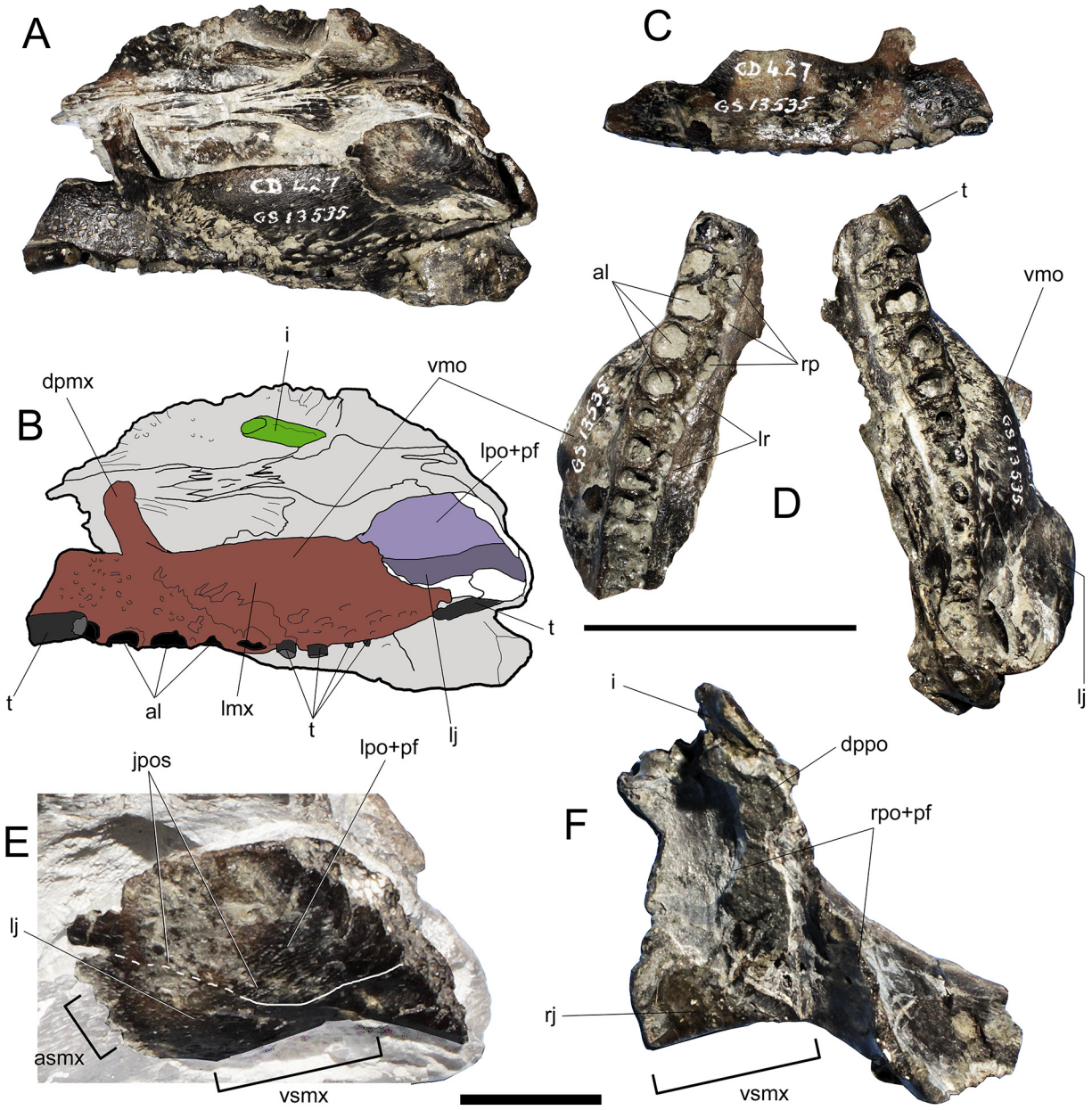

Fig. 3. CD 427. *Tuarangisaurus keyesi* Wiffen and Moisley 1986, referred juvenile individual. **A**. Left cheek elements in lateral view. The skull roof lies below the maxillary and postorbital, and is seen in dorsal view. **B**. Schematic of the elements illustrated in **A**. **C**. Right maxillary in labial view. **D**. Both maxillaries in ventral view, anatomically oriented with the alveoli in occlusal direction. **E**. Detail of the anterior part of the left jugal and postorbital + postfrontal, articulated, in external view. **F**. Detail of the posterior part of the right jugal and most of the postorbital + postfrontal, in internal view. **Anatomical abbreviations: acs**, anterior sutural contact with the squamosal; **al**, alveoli; **asmx**, anterior sutural contact with the maxillary; **dpmx**, dorsal process of the maxillary; **dppo**, dorsal process of the postorbital; **i**, indeterminate; **jpos**, jugal-postorbital suture; **lj**, left jugal; **lmx**, left maxillary; **lpo+pf**, left postorbital + postfrontal; **lr**, lingual ridge; **rj**, right jugal; **rp**, resorption pits; **rpo+pr**, right postorbital + postfrontal; **t**, tooth; **vmo**, ventral margin of the orbit; **vsmx**, ventral sutural contact with the maxillary. A-D, Scale bar equals 50 mm. E, F, scale bar equals 10 mm.

Postcranial Elements—A few postcranial elements are present in two separate blocks. One of them includes remains of five dorsal vertebrae (Fig. 8A). The three central elements are fairly complete, while the anteriormost is broken and only represented by its neural spine. The posteriormost vertebra in the block preserves half of its centrum and its neural spine. The vertebrae have massive and blunt transverse processes, with relatively short neural spines. From the top of the neural canal, the neural spines represents 2/5 of the whole vertebral height. In lateral view (Fig. 8A) the neural spines have a nearly square shape, being dorsoventrally short and laterally thick, ending in a flattened dorsal surface. An additional, separate block includes part of two other dorsal vertebrae, with similar features. The articular facet of the visible centrum is oval, being broader than high. Also, its neural canal is broader than high. Fragments of a rib and a gastralium are included in the same block (Fig. 8B, C). The rib is proximally thick and it has a rounded cross-section. On the other hand, the gastralium shows compact bony tissue in cross-section. The latter has an oval outline. It is likely dorsoventrally compressed; however, its orientation is uncertain. In the same block, two fragments of large, flattened bones are visible in cross section, being likely consistent with the pectoral girdle, based on their positions. The block also includes at least 23 visible gastroliths, ranging from smaller pebbles of about 5 mm diameter, to larger, oval and flattened stones over 30 mm in diameter (Fig. 8B,

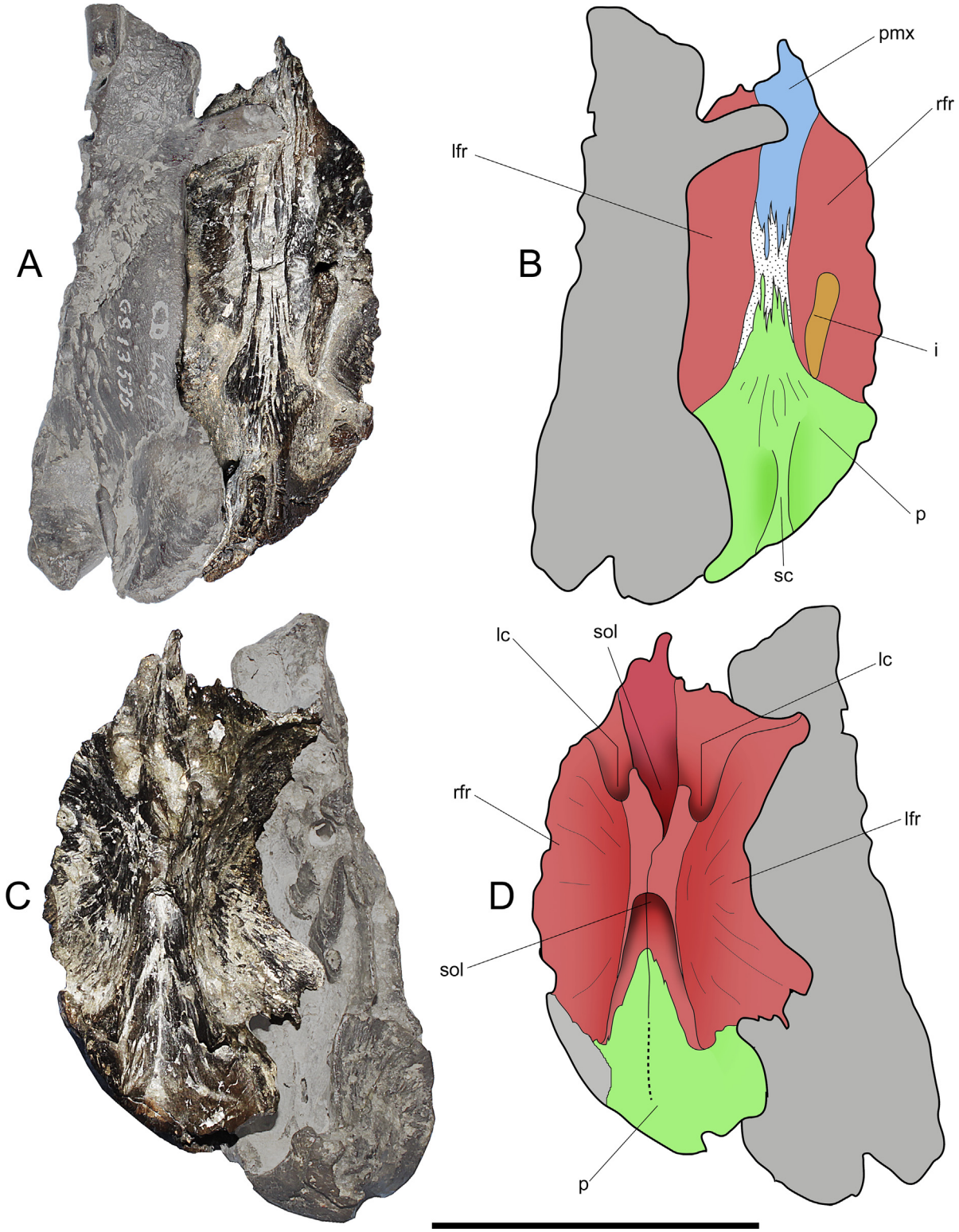

Fig. 4. CD 427. *Tuarangisaurus keyesi* Wiffen and Moisley 1986, referred juvenile individual. **A**–**B**. Dorsal aspect of the skull roof over the orbits. A, photo; B, schematic diagram. **C**–**D**. Ventral view of the skull roof below the orbits. C, photo; D, schematic of the elements illustrated in D. **Anatomical abbreviations: i**, indeterminate; **lc**, lateral concavities; **lfr**, left frontal; **p**, parietal; **pfr**, prefrontal (indeterminate laterality); **pmx**, premaxillary; **rfr**, right frontal; **sc**, sagittal crest; **sol**, *sulcus olfactorius*. Scale bar equals 50 mm.

C). Several other trunk elements are also preserved, including at least ten right dorsal ribs (Fig. 9A–C) and three ribs from the left. Seven anterior dorsal right ribs are articulated. These have circular cross-sections. Laterally, their distal ends converge to a common point. The posterior dorsal ribs (Fig 9B, C) have circular proximal cross-sections, while their distal part becomes flattened and reduced in diameter. A few limb elements are attached to the same block (Fig. 9C) including an indeterminate epipodial, one carpal or

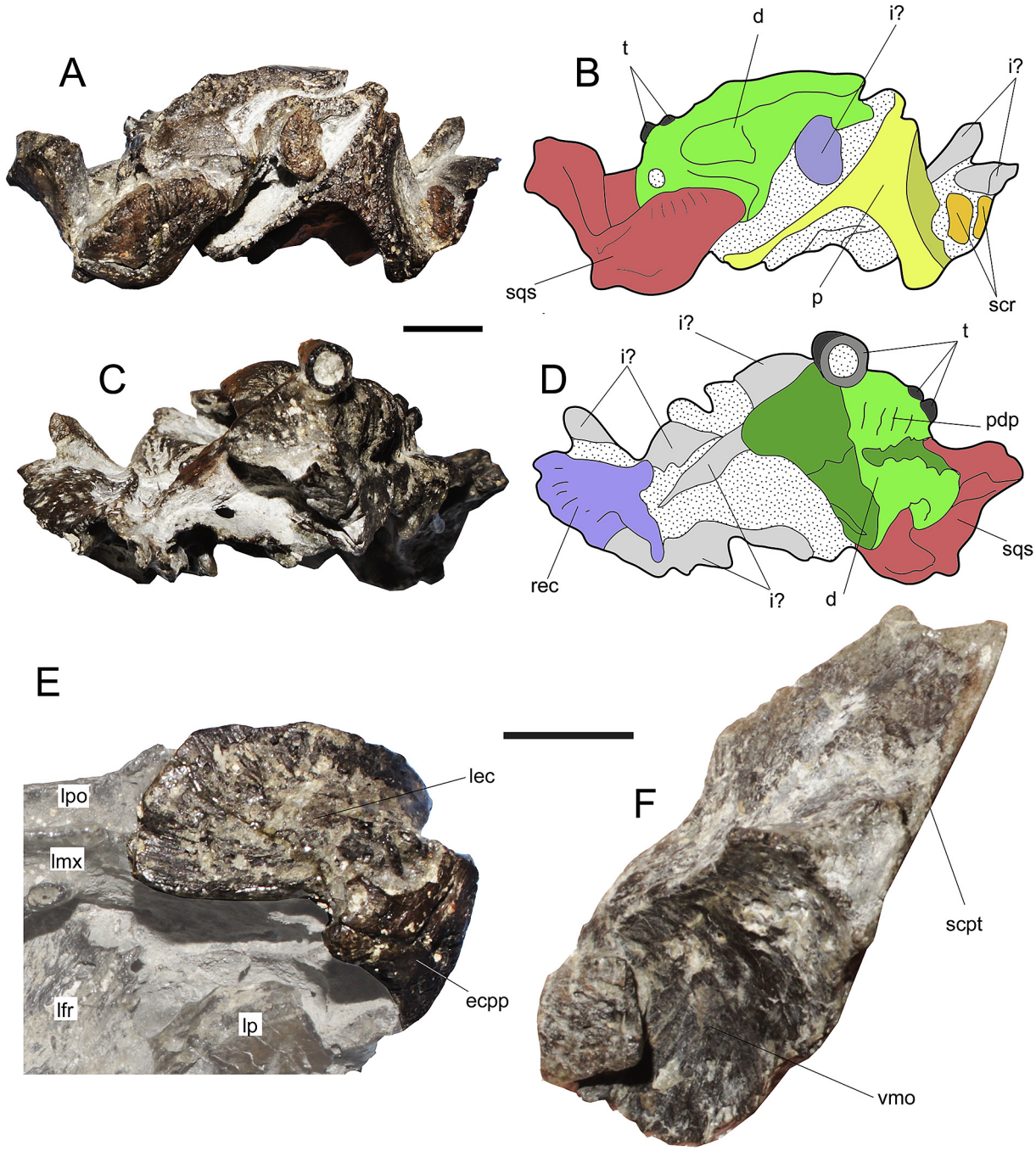

Fig. 5. CD 427. *Tuarangisaurus keyesi* Wiffen and Moisley 1986, referred juvenile individual. **A**–**B**. Crushed skull elements associated in a single block. A, photo; B, schematic diagram. **C**–**D**. Opposite view of the same block. C, photo; D, diagram. **E**. Left ectopterygoid in ventromedial view. **F**. Left palatine in dorsal view. **Anatomical abbreviations: d**, dentary; **ecpp**, ectopterygoid posterior process; **i?**, indeterminate; **lec**, left ectopterygoid; **lp**, left parietal; **lfr**, left frontal; **lmx**, left maxillary; **lpo**, left postorbital; **p**, parietal; **pdp**, paradental plate; **rec**, right ectopterygoid; **scpt**, suture contact with the pterygoid; **sqs**, squamosal socket for the quadrate; **t**, teeth; **vmo**, ventral margin of the orbit. Scale bar equals 10 mm.

tarsal element, and two metacarpal or metatarsals. Because of the young stage of the specimen and the lack of defined facets, it is difficult to determine the anatomical position of these elements, including if they belong to a back- or forelimb.

The left coracoid is also preserved (Fig. 9D). Its anterior half is massive, dorsally convex, with a biconvex symphyseal profile. A mid ventral process is not observed, likely because its early ontogenetic stage. Both the glenoid and scapular facets are poorly differentiated. In the anteromedial part, an anterior process, common among elasmosaurids, is already present. The posterior half of the coracoid is much narrower, with a poorly defined outline. The cordiform fenestra is widely open in the midline.

CD 427 also preserves one fairly complete limb. This is here considered as a forelimb (see Discussion), as previously pointed out by Wiffen and Moisley (1986). The propodial has an incomplete articular head. The articular surface is larger over the dorsal side of the propodial (see Discussion). This is interpreted as the composite articular surface of the head plus the tuberosity, the latter poorly differentiated in early growth stages. The shaft is massive and its distal extension is ca. 150% the size of the articular head. The distal

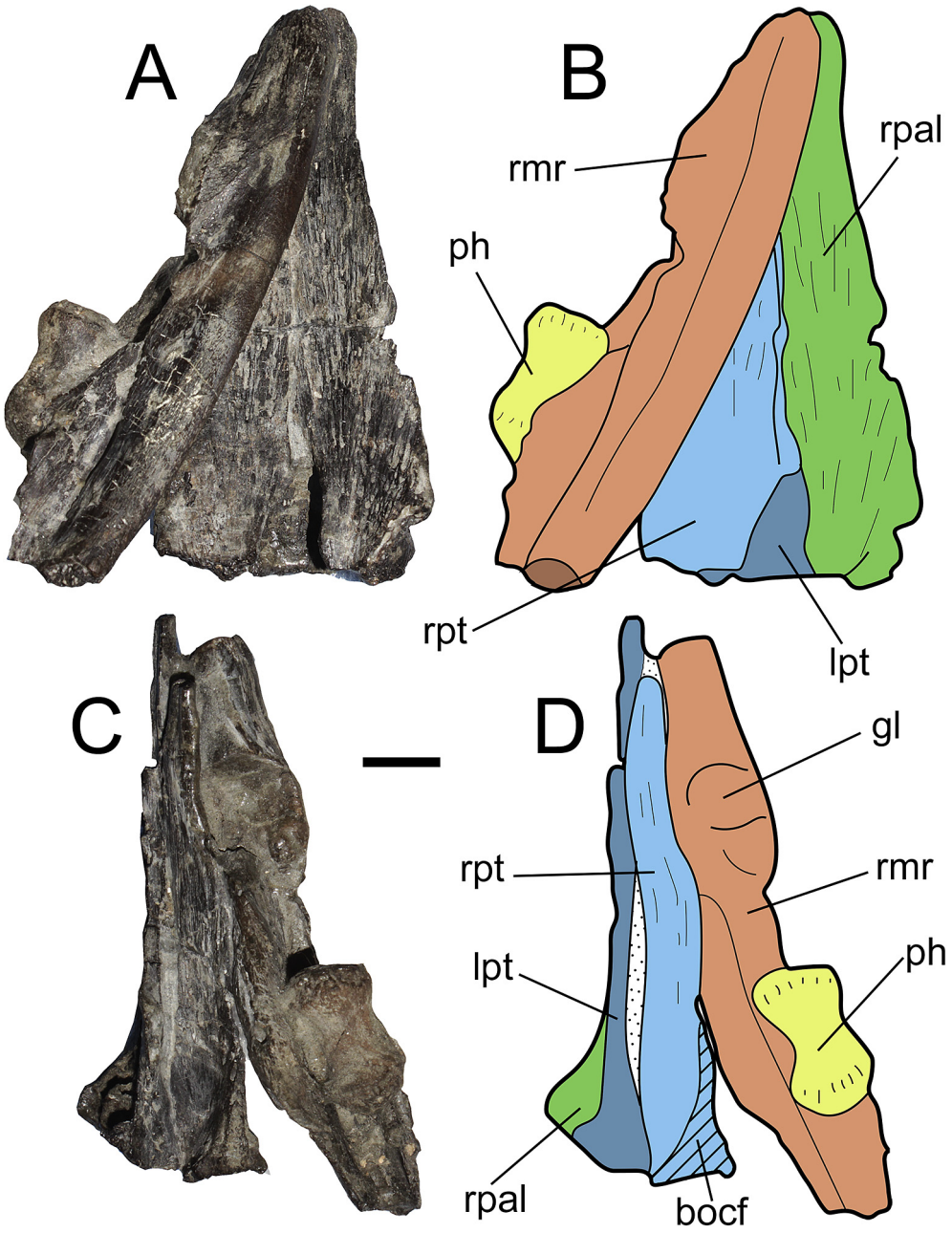

Fig. 6. CD 427. *Tuarangisaurus keyesi* Wiffen and Moisley 1986, referred juvenile individual. **A**. Ventral view of the right pterygoid and right palatine, attached to the right mandibular ramus. **B**. Schematic of the elements illustrated in A. **C**. Same block showing the right pterygoid in ventromedial view. **D**. Schematic of the elements illustrated in C. **Anatomical abbreviations: bocf**, basioccipital facet; **gl**, glenoid of the ramus; **lpt**, left pterygoid; **ph**, phalanx; **rmr**, right mandibular ramus; **rpal**, right palatine; **rpt**, right pterygoid. Scale bar equals 10 mm.

end lacks differentiated facets, appearing as a rounded, thick margin. A new arrangement is proposed here (Fig. 9E), reassessing the propodial orientation. The larger epipodial is interpreted here as the radius, being larger than the ulna. Both are rounded and lack any defined articular facets. The ulnare, centrale and radiale also lack differentiated articular facets. While the ulnare is slightly rounded, the centrale and the radiale are craniocaudally elongated.

6. Discussion

Referral of CD 427 to Tuarangisaurus keyesi—CD 427 shares several features with CD 425 and 426, holotype of *Tuarangisaurus keyesi* (Fig. 10). The ectopterygoid of CD 427 has a posteroventral process (Fig. 5E) very similar to that present on the holotype of *T. keyesi*, and recognized through CT-Scan (O'Gorman et al., 2017: fig 8D, E). Additionally, both specimens possess a convex ventral orbital margin formed by the maxilla. Although, this is present in other elasmosaurids (Welles, 1952; Carpenter, 1999), in both studied skulls this convex margin of the maxilla also extends laterally, forming the ventrolateral cup of the orbit. The ventral part of both maxillae even have a similar pit pattern (Fig. 10A). Also, in both specimens, the posterior extension of the maxilla fades with identical topology below the jugal and the postorbital + postfrontal complex (Fig. 10A, B). In the anterior part, the maxilla of both specimens also forms the ventral and posterior end of the external naris, and both have a straight anterior margin for contacting with

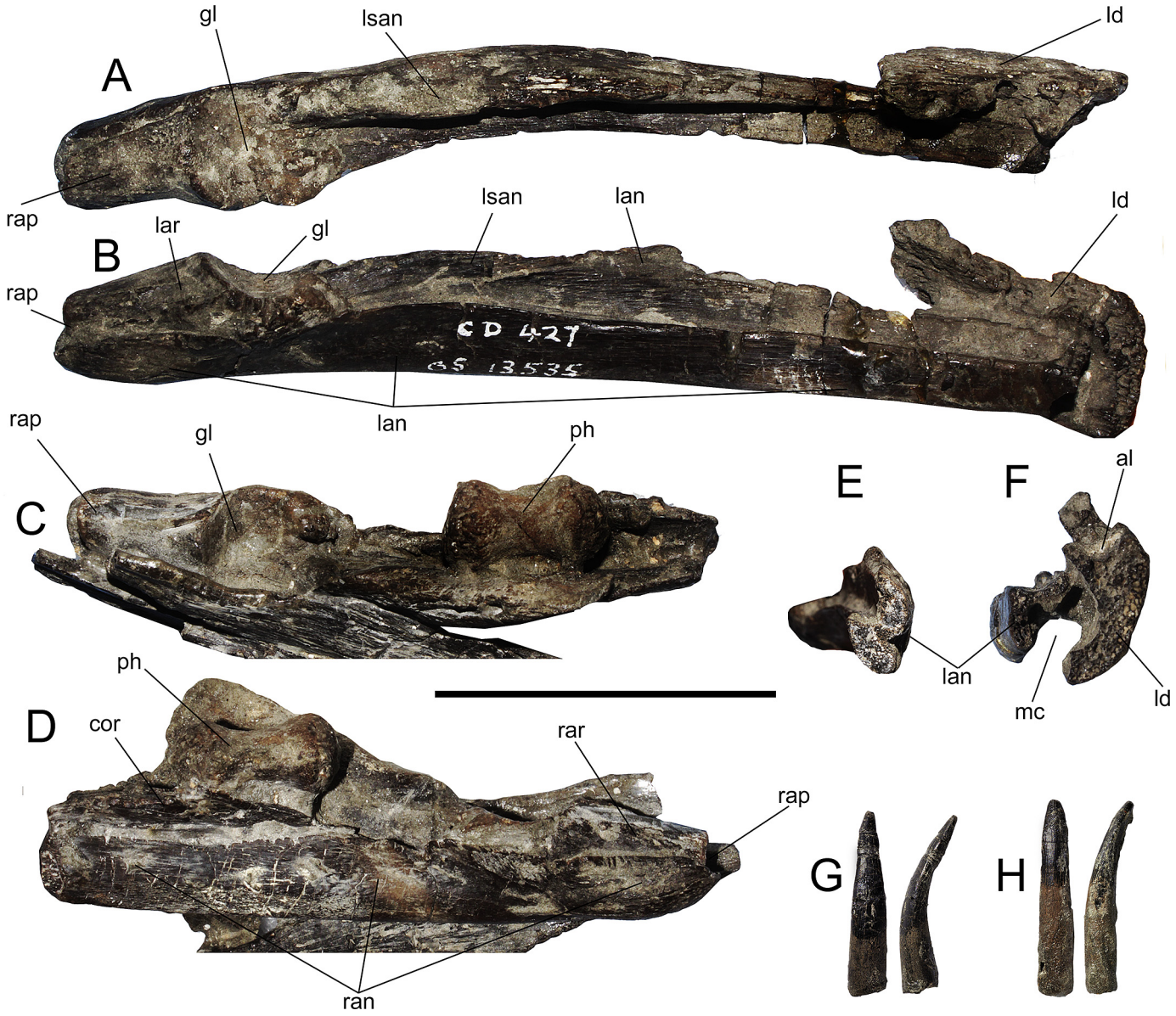

Fig. 7. CD 427. *Tuarangisaurus keyesi* Wiffen and Moisley 1986, referred juvenile individual. Mandibular elements. **A**–**B**. Posterior part of the left mandibular ramus in A, dorsal, and B, lingual views. **C**–**D**. Posterior part of the right mandibular ramus in C, dorsal, and D, ventrolingual views. **E**. Cross-section of the left surangular. **F**. Cross-section view of the anteriormost preserved portion of the left mandibular ramus. **G**, **H**, isolated teeth in labial and profile views, respectively. **Anatomical abbreviations: al**, alveolus; **cor**, coronoid; **gl**, glenoid; **lan**, left angular; **lar**, left articular; **ld**, left dentary; **lsan**, left surangular; **mc**, Meckellian canal; **ph**, phalanx; **ran**, right angular; **rap**, retroarticular process; **rar**, right angular. Scale bar equals 50 mm.

the premaxilla. The unique clear maxillar differences are observed in the dorsal narial process and the alveolar count (Fig. 10A). While in CD 427 the narial dorsal process is recurved rostrally, in CD 425 this is recurved caudally. In CD 427, the dorsal processes are not deformed, considering that the same condition is observed in both maxillae. However, a change in the angle of the dorsal process is likely related to ontogeny. Also, the alveolar count of CD 427 is 13 in the right maxilla and 14 in the left one. Wiffen and Moisley (1986: p. 210) estimate for the CD 425 adult skull a total of 15–16 maxilla teeth. The minimal difference of one or two teeth could be explained by tooth replacement as well as by the different ontogenetic stage of each specimen. Otherwise, the remaining maxillar features of both specimens are very similar. Moreover, the internal (ventral) view of the frontals in CD 427 confirms that the olfactory duct is formed by the frontals (Fig. 10C). In dorsal view, the posterior extension of the premaxilla reaches the parietal; however, the frontals are contacted in the midline, but dorsally covered by the posterior process of the premaxilla. The olfactory duct is formed by the frontals in the holotype of *T. keyesi* (CD 425), as previously noted by O'Gorman et al. (2017) through CT-Scan.

Both specimens also have a postorbital + postfrontal with its central part nearly square (Fig. 10B). In both specimens, the postorbital + postfrontals also have a dorsal process that extends over the posterior margin of the orbit. Also, the posterior process of the jugal is confined in both specimens by the maxilla and the squamosal, reaching the occlusal margin posterior to the maxilla. CD 427 has a premaxillae/parietal contact through an interdigitated suture that precludes the dorsal contact between frontals. This suture is lost in the adult CD 425. In the latter, the surface where the premaxillae and the parietal contact is very rugose, condition also

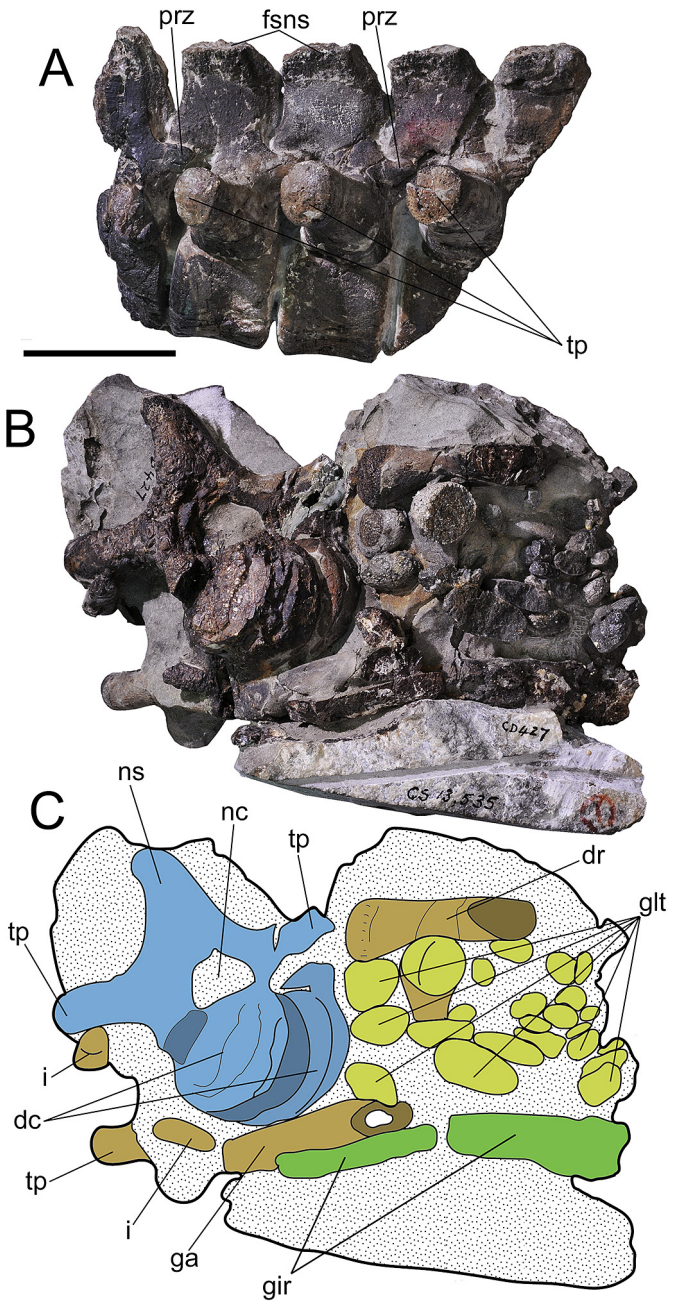

Fig. 8. CD 427. *Tuarangisaurus keyesi* Wiffen and Moisley 1986, referred juvenile individual. Postcranial elements. **A**. Articulated dorsal vertebrae in right lateral view. **B**. Block with trunk elements. **C**. Schematic of the elements illustrated in **B**. **Anatomical abbreviations: dc**, dorsal centra; **dr**, dorsal ribs; **fsns**, flattened dorsal surface of neural spines; **ga**, gastralium; **gir**, girdle fragments; **glt**, gastroliths; **i**, indeterminate; **nc**, neural canal; **ns**, neural spine; **prz**, prezygapophysis tp, transverse process. Scale bar equals 50 mm.

observed in the juvenile CD 427. Also, part of the anterior margin of the right temporal fossa is preserved on CD 427, and shares a very similar outline with that of CD 425. Finally, the pterygoids of CD 427 have a triradiate shaft in posterior view (Fig. 10D). This condition is also present in CD 425. Furthermore, the outline of the basioccipital facet present in CD 427 pterygoid is almost identical to that of CD 425. In addition, CD 426 is an articulated squamosal, quadrate and posterior mandibular ramus, plus a cervical series which are included in the holotype of *T. keyesi*. These have been considered as part of the same skull CD 425. Although no highly diagnostic features are present in this portion, the morphology of CD 426 is consistent with the posterior part of the mandibular rami of CD 427.

All these parallel anatomical features strongly support CD 427 as congeneric and conspecific with CD 425 and 426. Minor morphologic differences can be attributed to the respective ontogenetic stage of each specimen. Therefore, CD 427 is here referred to *T. keyesi*.

Previous referral of CD 427 to Aristonectinae indet.—Araújo et al. (2015) included CD 427 in two different phylogenetic analyses, recovering this specimen within the Aristonectinae. The first analysis considered four new specimens from Angola, plus MML-PV5 from Argentina (Aristonectinae indet. in O'Gorman et al., 2014) and CD 427, all within a single Operational Taxonomic Unit (OTU). However, these authors omitted the fact that CD 427 preserves cranial elements, and a few of these elements were already described by Wiffen and Moisley (1986: p. 215 and figs. 7-12). The maxillary of CD 427 has 13 or 14 teeth, indicating beyond any reasonable doubt that this specimen is a non-aristonectine elasmosaurid, contrary to the 50 or more maxillary teeth present in *Aristonectes* spp., *Morturneria seymourensis* and *Kaiwhekea katiki*. Because of this, CD 427 cannot be considered as an equivalent OTU with MML PV5. The latter is indeed an aristonectine with remarkable postcranial similarities to SGO.PV.260 (juvenile referred to *Ar. quiriquinensis*). Therefore, the first phylogenetic results of Araújo et al. (2015) using this merged OTU needs to be reviewed under these considerations. The second analysis considered CD 427 as a separate OTU. This was recovered as the sister taxon of the Angolan OTU, and both were recovered in polytomy, as a sister clade of *Aristonectes* and *Kaiwhekea*. Because of this polytomy, the relationships between aristonectines and the Angola specimens + CD 427 cannot be assured. Summarizing, the phylogenetic analysis of Araújo et al. (2015) is not conclusive regarding the taxonomy of CD 427, and moreover, these authors omitted very relevant cranial information that demonstrates CD 427 is a non-aristonectine.

Assessment of cranial elements with uncertain anatomical identity—Wiffen and Moisley (1986) noted a number of sutures on the holotype of *T. keyesi*, but stated that the individual cranial bones were difficult to determine. These authors correctly identified the premaxilla-maxilla suture, the sutures of the elements surrounding the anterodorsal part of the orbit (regarding them as maxilla and prefrontal or frontal), and the posterior downturned rod of the maxilla with the jugal. O'Gorman et al. (2017) provided emerging information from CT-Scans of the CD 425 skull. The latter study confirmed the straight premaxilla-maxilla suture that reaches between the orbits. It also recognized the presence of a separate element in the anterodorsal margin of the orbit, between the maxillary and the dorsal process of the premaxilla. This element was then identified as the frontal (O'Gorman et al., 2017: fig. 7.1). The posterior contact of this element still had an obscure outline. The posterior part of the orbit was considered by these authors as formed dorsally by the frontal, medially by the postorbital + postfrontal, and ventrally by the anterior extension of the jugal, the postorbital, and part of the maxilla (O'Gorman et al., 2017: fig. 7A). A similar topology is here recognized in CD 427, however, the outlines of the postorbital and postfrontal cannot be determined because of the early fusion of both elements.

The emerging interpretation here based on skull ontogeny allows us to emend a few previous considerations. The suture between the premaxilla and the parietal is obscured in the CD 425 skull, while CT scan could not accurately resolve the outline of each bone. Based on the open premaxilla/parietal contact present in CD 427, we can find a very light, however, still visible contact between both elements in the CD 425 skull. The interpretation is difficult because the interorbital surface is very rugose. The contact of both elements is settled over the anterior half of the orbit. The juvenile

Fig. 9. CD 427. *Tuarangisaurus keyesi* Wiffen and Moisley 1986, referred juvenile individual. Postcranial elements. **A**. Articulated anterodorsal ribs in dorsal view. **B**. Articulated posterodorsal ribs in dorsal view. **C**. Same in ventral view. **D**. Left coracoid in dorsal view. **E**. Articulated left forelimb in ventral view. **Anatomical abbreviations: ah**, articular head; **ap**, anterior process of the coracoid; **c/t**, carpal/tarsals; **cf**, cordiform fenestra; **ce**, centrale; **drb**, dorsal ribs; **ep**, epipodial; **ga**, gastralia; **gl**, glenoid; **h**, humerus; **mc/mt**, metacarpals/metatarsals; **ra**, radius; **rd**, radiale; **scf**, scapular facet; **sy**, symphysis **ue**, ulnare; **ul**, ulna. Scale bar equals 50 mm.

CD 427 confirms that the dorsal contact between the frontals is precluded by the premaxilla/parietal contact, as previously pointed out by O'Gorman et al. (2017). However, the ventral view of CD 427 shows that both frontals are indeed contacted below the premaxilla/parietal dorsal contact, as previously noted by O'Gorman et al. (2017) based on the CT scans of the holotype. In dorsal view of CD 425 skull, the frontals can be anteriorly tracked to near 10 mm posterior to the external naris, without entering its margin. Part of the anterior extension of the left prefrontal is likely lost due to the original preparation with acetic acid, leaving a small triangular gap

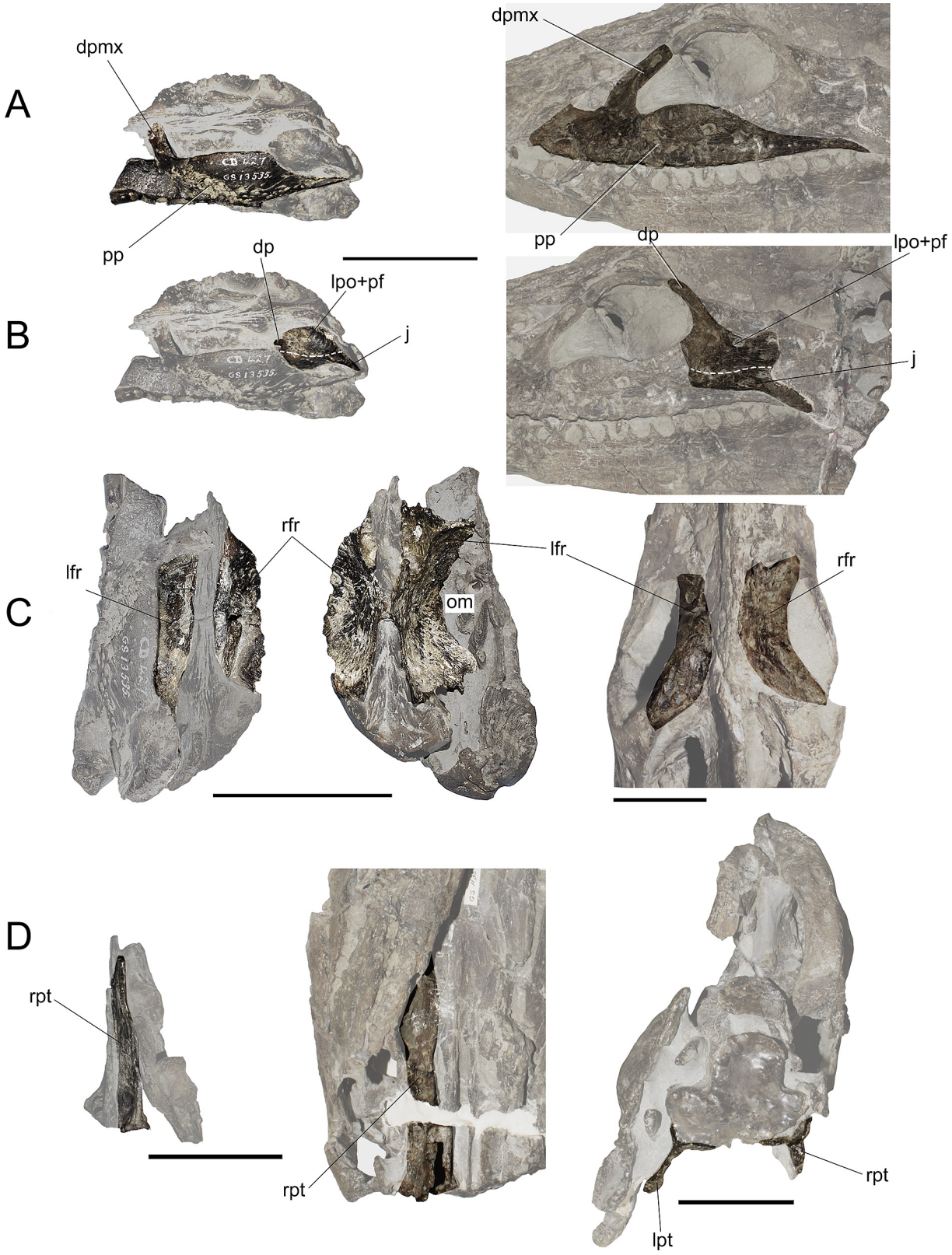

Fig. 10. Comparison between juvenile skull CD 427 and CD 425 + 426, holotype of *Tuarangisaurus keyesi* Wiffen and Moisley, 1986. **A**. From left to right: CD 427 (left) and CD 425 (holotype, right) in left lateral view, remarking the maxillary. **B**. From left to right: CD 427 and CD 425 (holotype, right) in dorsal view, respectively, remarking the postorbital + prefrontal. **C**. From left to right: CD 427 in dorsal view, CD 427 in ventral view, and CD 425 (holotype) in dorsal view, remarking the frontals. **D**. From left to right: CD 427 pterygoid in ventromedial view, CD 425 (holotype) pterygoid in ventral view, and CD 425 pterygoid in occipital view, showing its triradiate shaft. **Anatomical abbreviations: dp**, dorsal process of the postorbital; **dpmx**, dorsal process of the maxillary; **j**, jugal; lfr, left frontal; **lpo**+**pf**, left postorbital + postfrontal; **lpt**, left pterygoid; **om**, orbit margin; **pp**, pit pattern; **rfr**, right frontal; **rpt**, right pterygoid. Scale bars equals 50 mm.

visible on the skull. The right frontal is partially covered by the lateral crushing of the skull. Both frontals are anteriorly disarticulated and slightly displaced dorsally, leaving a separation with the dorsal narial process of the maxilla.

The interpretation of elements posterior to the orbit can also be emended. Based on the juvenile CD 427, its clear maxilla/jugal contact allows us to assess the same contact in CD 425. Thus, the anterior process of the squamosal does not reach the posterior margin of the orbit, which is fully enclosed by the maxilla and jugal. Its jugal develops a ventroposterior process over the posterior extension of the maxilla. This disappears posteriorly under the jugal. Finally, the osteologic and ontogenetic evidence suggests that the putative frontal foramen noted by O'Gorman et al. (2017) is not an actual anatomical feature, but an artifact of the original preparation with acetic acid (Wiffen and Moisley, 1986). The pterygoids were also partially lost during acid preparation. All these observations are summarized in our reinterpretation of the skull sutures (Fig. 11).

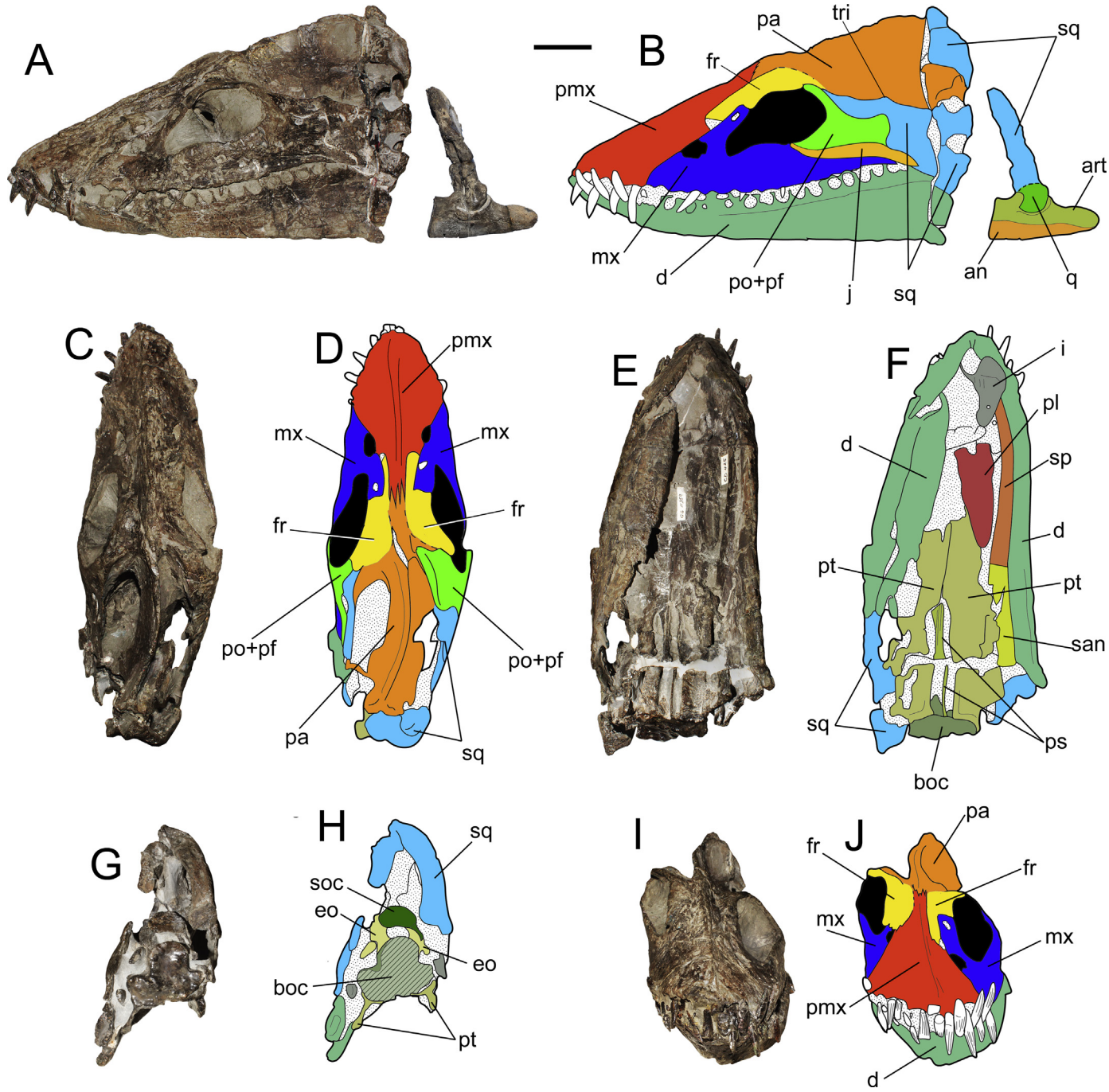

Fig. 11. CD 425 + 426. *Tuarangisaurus keyesi* Wiffen and Moisley, 1986. Holotype. Anatomical identification of the skull elements **A**. CD 425 + 426 in left lateral view. **B**. Schematic of the elements illustrated in **A**. **C**. Dorsal view of the skull. **D**. Schematic of the elements illustrated in **C**. **E**. Ventral view of the skull. **F**. Schematic of the elements illustrated in **E**. **G**. Posterior (occipital) view of the skull. **H**. Schematic of the elements illustrated in **G**. **I**. Anterior view of the skull. **J**. Schematic of the elements illustrated in **I**. **Anatomical abbreviations: an**, angular; **art**, articular; **boc**, basioccipital; **d**, dentary; **eo**, exoccipital-opistothic; **fr**, frontal; **i**, indeterminate; **l**, jugal; **mx**, maxilla; **pa**, parietal; **pl**, palatine; **pmx**, premaxilla; **po**+**pf**, left postorbital + postfrontal; **ps**, parasphenoid; **pt**, pterygoid; **q**, quadrate; **san**, surangular; **soc**, supraoccipital; **sp**, splenial; **sq**, squamosal; **tri**, temporal ridge. Scale bars equals 50 mm.

New anatomical features of T. keyesi—The juvenile CD 427 studied here shows that the angular of *T. keyesi* is a long bone estimated to extend from the retroarticular process (together with the articular) as far as the first posterior teeth, based on the presence of an attached dentary fragment on the left mandibular ramus. The angular has a lingual, deep sulcus that ends just before the anterior preserved part of the bone (which is anteriorly incomplete). This sulcus is consistent with the articular surface for the coronoid. The latter was confirmed as a dorsoventrally high bone, based in a fragment recognized by O'Gorman et al (2017: fig. 9J-M).

Another interesting CD 425 feature is the presence of a small dorsal prominence of the jugal bar. Such structure was previously noted in the North American, Late Cretaceous genus *Styxosaurus* and identified as a temporal ridge (Otero, 2016). Assessing the growth pattern of the jugal, from the young condition in CD 427 and the adult condition with well-developed processes in CD 425, it is likely that the temporal ridge could be linked to the growth of the posterodorsal margin of the jugal, causing a dorsal displacement of the squamosal; this is reflected in a small prominence over the margin of the temporal fossa.

Even in its immature condition, the dorsal vertebrae of CD 427 allow us to observe that their neural spines are short and blunt, with thick transverse processes horizontally oriented. The anterior outline of the dorsal centra are oval. All these features have been described for young aristonectines from the Upper Cretaceous of South America (Otero et al., 2012; O'Gorman et al., 2014). Unequivocally, CD 427 is a non-aristonectine elasmosaurid. This shows that such dorsal features are indeed present both in young aristonectines, as well as in young, austral non-aristonectine elasmosaurids. Interestingly, when compared with Late Cretaceous, very young elasmosaurids from North America such as AMNH 5261 (holotype of '*Leurospondylus ultimus*' Brown, 1913), these features observed in dorsal vertebrae of Weddellian elasmosaurids are not present. This could suggest a possible common ancestor for austral non-aristonectines as well as for aristonectines, because a very similar morphotype of dorsal vertebrae is present in very juvenile specimens of both groups, having also biogeographic and chronostratigraphic affinities. The latter relationships have been assessed by O'Gorman and Coria (2016) with the proposal of the clade Weddellonectia, although *T. keyesi* was not recovered as part of the Weddellonectia. The forelimb of CD 427 also provides relevant information. The epipodials of the *T. keyesi* forelimb are unequivocally broader than long. The same condition also occurs in the centrale and radiale.

In addition, the positive determination of CD 427 as *T. keyesi* allows us for the first time to shed light on the juvenile postcranial skeleton of this species. The adult postcranial skeleton was first restricted only to its holotype comprising the skull and anterior cervicals. More recently, Hiller et al. (2017) reassessed the specimen CM Zfr 115 from upper Campanian levels of Conway River, North Canterbury, New Zealand. This is a fairly complete skeleton, found by the latter authors as referable to *Tuarangisaurus* sp. An accurate comparison between CD 427 and CM Zfr 115 is difficult because of the different ontogenetic stage of each specimen. However, both specimens share distinctive features, among them, very similar mandibular rami with similar glenoids and retroarticular processes; presence of dorsal vertebrae with thick, horizontal diapophyses and dorsoventrally compressed neural canal; thick ribs with circular cross-section; forelimbs with epipodials mesiodistally shorter than craniocaudally broad, and mesiodistally short and dorsoventrally compressed phalanges. None of these elements are diagnostic enough for genus determination, however, the common combination of features in CD 427 and CM Zfr 115 postcranial skeletons do not contradict a possible congenerity.

Orbital Changes Through Ontogeny—As previously indicated, the unique major difference between the maxillae of CD 425 and 427 is the orientation of the narial dorsal process. As is documented in several extant Reptilia (and Amniota), the proportion between the skull and the orbit size varies during the ontogeny (Romer, 1956; Carroll, 1988). Skull ontogenetic series of the genera *Crocodylus*, *Caiman*, and *Alligator* shows that the orbits are very large with respect to the whole skull in young individuals, reaching between one quarter and one-third of the skull length, while in adult specimens is between one-sixth to one-eighth the skull length (Mook, 1921). A similar condition is documented in Squamata, particularly in *Varanus panoptes*. In very young individuals, the orbit reaches ca. one-third the skull length, while in adults, this reaches near one-fifth the skull length (Werneburg et al., 2015). Therefore, it is expected that the orbit of elasmosaurids underwent similar ontogenetic changes. In this way, the angle variation of the dorsal narial process of the maxilla could be explained by a progressive elongation of the skull, with a comparatively arrested orbital growth (Fig. 12A–C), as happens in several extant reptiles.

Anatomical interpretation of the anteroventral orbital notch—Among other characters, the reniform orbit outline (caused by a dorsal convexity of the maxilla into the orbit) was considered by Benson and Druckenmiller (2014) as a synapomorphy of Xenopsaria. However, similar structures are present in non-xenopsarian cryptoclidians. Particularly, the cryptoclidid *Vinialesaurus caroli* (Gasparini et al., 2001) from the Oxfordian of Cuba, displays a similar orbit outline (Gasparini et al., 2001: fig. 2C). This trait also disappears in few elasmosaurids such as *Futabasaurus suzukii* Sato et al., 2006, and likely in *Libonectes morgani* (Welles, 1949), however, this portion of the skull is damaged in the latter. Thus, the reniform orbit is present outside Xenopsaria, while within Xenopsaria, it is absent in a few representatives. The leptocleidian *Nichollsaura borealis* Druckenmiller and Russell, 2006 also has a similarly shaped orbit but this is formed by a cranial extension of the jugal.

The ontogenetic series of *T. keyesi* studied here suggests that the anteroventral orbital notch is progressively excavated during growth as a consequence of the posterodorsal migration of the narial dorsal process of the maxilla. Interestingly, in ventral view, CD 427 frontals have two lateral concavities on each side of the *sulcus olfactorius*. These concavities occur immediately adjacent to the place where the orbital notch will be developed in the adult stage. Considering the placement of the two internal, lateral concavities below each frontal of *T. keyesi*, and the adjacent occurrence of the orbital anterior notch, these facts suggest that a gland (likely a salt gland) could occur in *T. keyesi* and moreover, it could be placed immediately anterior to the eye ball, and within the orbital margin. This same condition could also be present in other plesiosaurians a with reniform orbital outline.

Anatomical identification of the CD 427 limb—The CD 427 extremity was treated as an indeterminate limb in its first description by Wiffen and Moisley (1986), although they did suggest it was a forelimb. The presence of the skull as well as dorsal elements of the trunk, plus the lack of any remains from the posterior skeleton, indirectly suggest that this extremity could indeed be anterior. The reconstructed position indicated by Wiffen and Moisley (1986: fig. 18) included a preaxial epipodial much larger than the postaxial epipodial. Such condition was previously described in forelimbs of austral non-aristonectines (Broili, 1930: fig. 1; Gasparini et al., 2003: fig. 4C; Hiller et al., 2005: fig. 15; Hiller et al., 2014: fig. 8).

On the other hand, the propodial lacks part of its articular head, but the articular surface is asymmetrically extended along the dorsal and ventral side of the diaphysis. On one side, as shown by Wiffen and Moisley (1986: fig. 18), this has a slight distal extension over the shaft, being also slightly displaced from the midline of the

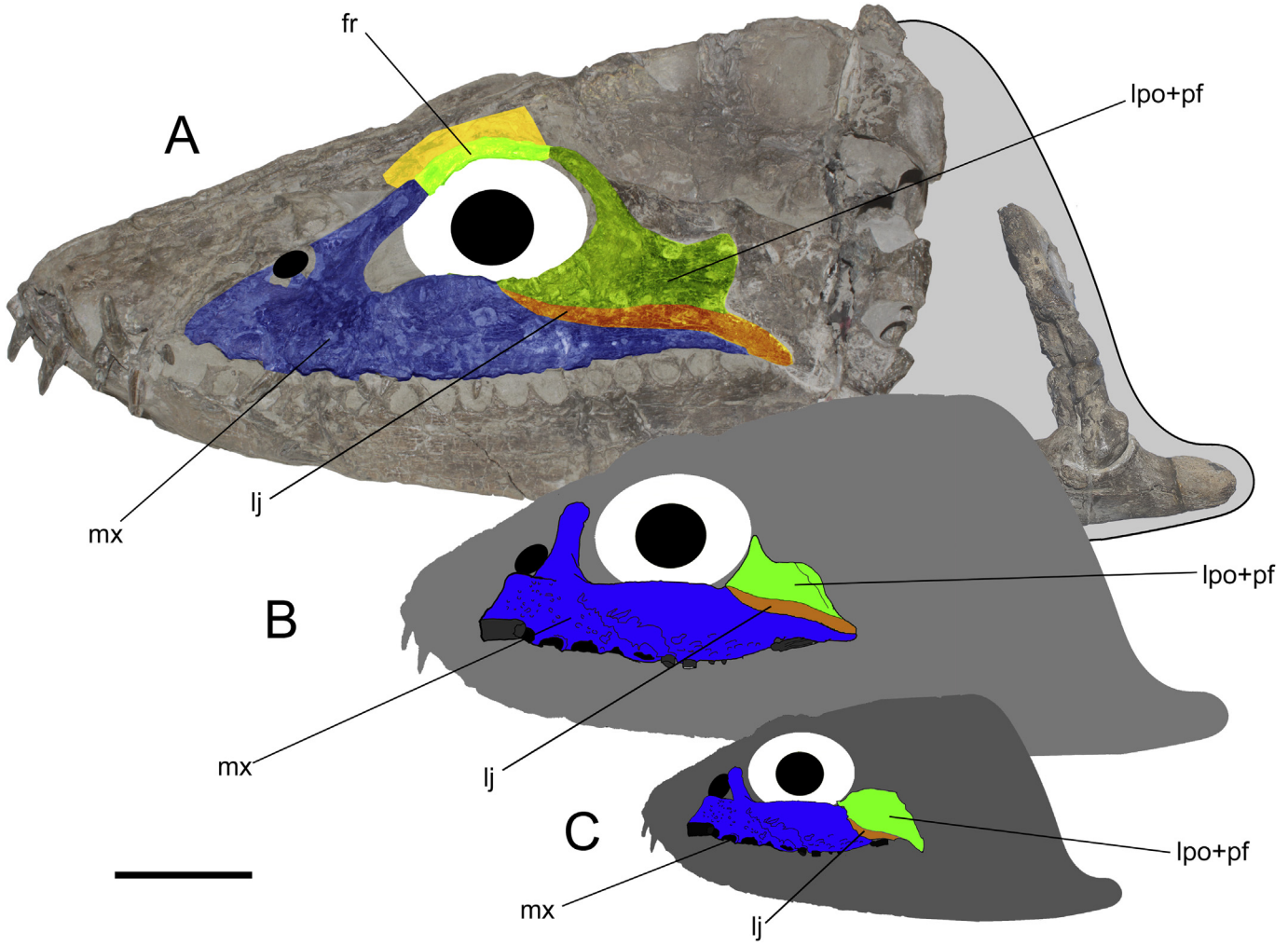

Fig. 12. Skull ontogeny and orbital changes in *Tuarangisaurus keyesi* Wiffen and Moisley 1986. **A**. Orbit anatomical elements of CD 425 + 426 (holotype) in left lateral view. **B**. Hypothetic expectable ontogenetic intermediate, in left lateral view. **C**. Orbit anatomical elements of CD 427, referred juvenile skull studied here. **Anatomical abbreviations: fr**, frontal; **lj**, left jugal; **lpo**+**pf**, left postorbital + postfrontal; **mx**, maxilla; Scale bars equals 50 mm.

shaft. Its opposite side is shorter and does not extend distally, at least based on the preserved portion. Such a condition was previously observed among other austral elasmosaurids (Otero et al., 2015: fig. 3). In the young stage, the proximal articular surface of the propodial appears as being extended into the shaft. At a later ontogenetic stage, the young articular surface is differentiated into the articular head and the tuberosity. Thus, the figure provided by Wiffen and Moisley (1986: fig. 18) likely shows the propodial in dorsal view. In adult elasmosaurids, the tuberosity is slightly shifted to the postaxial margin (Welles, 1952, 1962). Then, based on this, the propodial is on the left side. In consequence, the available extremity can be identified as a left extremity, likely a forelimb, based on the trunk portion preserved.

Remarks about dorsal features—The features of the dorsal vertebrae of CD 427 are also present in known juvenile aristonectine skeletons such as SGO.PV.260 (*Aristonectes quiriquinensis*, juvenile referred) from the upper Maastrichtian Quiriquina Formation of central Chile (Otero et al., 2012)and MML PV 5 (former holotype of *Tuarangisaurus*? *cabazai* and currently considered as Aristonectinae indet.) from the upper Maastrichtian Jagüel Formation of Argentinean Patagonia (Gasparini et al., 2003; O'Gorman et al., 2014). Indeed, the dorsal vertebrae of CD 427 are almost undistinguishable from equivalent elements of these two South American specimens. SGO.PV.260 shows an anterior keel in the neural spine (Otero et al., 2012: fig. 5B), which seems to be less defined in MML PV 5 (O'Gorman et al., 2014: fig. 2K, L). However, this feature cannot be assessed in CD 427 because the available dorsal centra remain articulated or they have their articular facets broken. Other postcranial elements show slight differences in their juvenile stage. Particularly, the coracoids of SGO.PV.260 and MML PV 5 have their posterior part comparatively larger than CD 427, and they have more defined glenoid and scapular facets than those of the CD 427 coracoid. The latter is very similar to another specimen (CD 428) referred by Wiffen and Moisley (1986: fig. 22 and 23) to aff. *T. keyesi*.

Comparison of CD 427 with other known juvenile plesiosaurian skulls—The absence of pineal foramen in CD 427 suggests that this trait is not ontogenetic. Even more, it seems to be a sinapomorphy of derived Elasmosauridae, considering its widespread presence in basal plesiosaurians, and in the Leptocleididae (sister taxon of Elasmosauridae), particularly in the juvenile holotype of *Brancasaurus wegneri* Wegner, 1914 (see Sachs et al., 2016: fig. 3).

On the other hand, the anteriorly recurved dorsal process of the CD 427 maxilla is similar to that observed in the juvenile skull of *Seleeyosaurus guilelmiimperatoris* (O'Keefe, 2004: fig. 2; Groβmann, 2007: fig. 4), from the Toarcian of Holzmaden; however, this element was interpreted as the prefrontal in the reconstruction proposed by Groβmann (2007 fig. 6). Another juvenile specimen

described by Vincent (2010: fig. 2), from the same age and locality, it shows a similar condition with the prefrontal forming the posterior margin of the external naris. Adding to this discussion, in the proposed reconstructions of *Cryptoclidus eurymerus* by Brown (1981: fig. 1) and *Tricleidus seeleyi* (Brown, 1981: fig. 22), these taxa show a dorsal process craniocaudally thick and dorsally short, with no suggested presence of a prefrontal. On the other hand, Sachs et al. (2016) provided a more accurate reconstruction of *Brancasaurus brancai*, indicating the presence of the prefrontal in the same topology of CD 427 maxillary dorsal process, and forming the posterior margin of the external naris. The commented specimens support that the process forming the bar between the external naris and the orbit, indeed belongs to the prefrontal; however, in the case of CD 427, there is no clear evidence of this process as separate element from the maxilla. Considering the presented evidence in several plesiosaurians, if these are indeed two separate elements, the fusion of both ocurred in earlier ontogenetic stages of *T. keyesi*.

7. Conclusions

The remarkable juvenile specimen CD 427 includes several informative skull elements, as well as a significant portion of the anterior trunk and left forelimb, which are assessed here in more detail than in the original description. Detailed study of this specimen revealed features in common with the holotype of *Tuarangisaurus keyesi* (CD 425 and 426). These include the dorsal contact between the premaxilla and parietals through a rugose dorsal surface, the presence of a well-marked maxillar lobe extended into the orbit, a similar pit pattern in the labial surface of the maxilla, a maxillar tooth number of approximately 14, a triradiate pterygoid shaft with a concave basioccipital articular facet, elongated posterior interpterygoid vacuities, and an ectopterygoid with a posterior process. However, a few differences have been addressed, particularly, the orientation of the narial dorsal process of the maxilla. Considering the arrested orbital growth with respect to the rest of the skull, as seen in several extant reptiles, it is likely that during the skull growth of *T. keyesi* a posterior recurving of this process occurred. There is a minor difference also in the tooth number of the maxilla, which can be a consequence of replacement as well as by the different ontogenetic stages of the studied specimen with respect to the *T. keyesi* holotype. Anatomically, all the other available skull topologies of CD 427 are comparable to those of the *T. keyesi* holotype. Therefore, we refer the juvenile specimen CD 427 to the same genus and species, being the first skull ontogenetic series available for a Late Cretaceous, austral elasmosaurid.

The visible sutures of the *T. keyesi* holotype skull, as noted by previous CT-Scan analysis, plus the juvenile skull studied here, allow us to propose a more accurate definition of the skull elements in the adult. Also, it provides a partial understanding of how the skull of non-aristonectine elasmosaurids could have grown. This research also provides the first insights into the trunk and forelimb of *T. keyesi*, at least based on the available juvenile specimen studied here. Dorsal vertebral features have been found to be remarkably similar to those of juvenile and adult aristonectines, suggesting that the dorsal axial skeleton of this latter clade is indeed, pedomorphic.

Acknowledgments

RAO was initially supported by the project Anillo de Ciencia Antártica ACT-105, 2010–2013, Conicyt – Chile, and later by Domeyko II UR-C12/1 grant–Red Paleontológica U-Chile of the Universidad de Chile. JPO was supported by projects PICT 2012-0748, UNLP N 677, UNLP N 607 and PIP 0433. J. Simes (GNS Science, Lower Hutt New Zealand), A. Tennyson and A. Kusabs (Museum of New Zealand Te Papa Tongarewa, Wellington, New Zealand) are acknowledged for granting access to the studied specimens. The authors want to thank two anonymous reviewers for their valuable comments and suggestions which improved the manuscript.

References

Araújo, R., Polcyn, M.J., Lindgren, J., Jacobs, L.L., Schulp, A.S., Mateus, O., Olímpio Gonçalves, A., Morais, M.L., 2015. New aristonectine elasmosaurid plesiosaur specimens from the early Maastrichtian of Angola and comments on paedomorphism in plesiosaurs. Netherlands Journal of Geosciences 94, 93–108.
Benson, R.B.J., Druckenmiller, P.S., 2014. Faunal turnover of marine tetrapods during the Jurassic–Cretaceous transition. Biological Reviews 89, 1–23.
Broili, F., 1930. Plesiosaurierreste von der Insel Quiriquina. Neues Jahrbuch Mineralogie Geologie Paläontologie Beilage-Band (B) 63, 497–514.
Brown, B., 1913. A new plesiosaur, *Leurospondylus*, from the Edmonton Cretaceous of Alberta. Bulletin of the American Museum of Natural History 32, 605–615.
Brown, D.S., 1981. The English Late Jurassic Plesiosauroidea (Reptilia) and review of the phylogeny and classification of the Plesiosauria. Bulletin of the British Museum (Natural History), Geology 4, 225–234.
Carpenter, K., 1999. Revision of North American elasmosaurs from the Cretaceous of the Western Interior. Paludicola 2, 148–173.
Carroll, R.L., 1988. Vertebrate Paleontology and Evolution. W H. Freeman and Company, New York, 711 pp.
Cope, E.D., 1869. Synopsis of the extinct Batrachia, Reptilia and Aves of North America. Transactions of the American Philosophical Society, New Series 14, 1–252.
Crampton, J.S., 1990. A new species of Late Cretaceous wood-boring bivalve from New Zealand. Palaeontology 33, 981–992.
Crampton, J.S., Moore, P.R., 1990. Environment of deposition of the Maungataniwha Sandstone (Late Cretaceous), Te Hoe River area, western Hawke's Bay, New Zealand. New Zealand Journal of Geology and Geophysics 33, 333–348.
Cutten, H.N.C., 1994. Geology of the middle reaches of the Mohaka River, 6. Institute of Geological and Nuclear Sciences Geological Map, 38 pp. 1 map.
de Blainville, H.M.D., 1835. Description de quelques espèces de reptiles de la Californie précédé de l'analyse d'un système général d'herpétologie et d'amphibiologie. Nouvelles Annales du Muséum d'Histoire Naturelle de Paris, Série 3–4, 233–296.
Druckenmiller, P.S., Russell, A.P., 2006. Anatomy of an exceptionally complete specimen of a new genus of plesiosaur from the Early Cretaceous (early Albian) of northeastern Alberta, Canada. Palaeontographica Abteilung A 283, 1–33.
Eagle, M.K., 1994. A new Upper Cretaceous species of *Isselicrinus* (Crinoidea: Articulata) from western Hawkes Bay, New Zealand. Records of the Auckland Institute and Museum 31, 175–186.
Feldmann, R.M., 1993. Additions to the fossil decapod crustacean fauna of New Zealand. New Zealand Journal of Geology and Geophysics 36, 201–211.
Gasparini, Z., Bardet, N., Iturralde-Vinent, M., 2001. A new cryptoclidid Plesiosaur from the Oxfordian (Late Jurassic) of Cuba. Geobios 35, 201–211.
Gasparini, Z., Salgado, L., Casadío, S., 2003. Maastrichtian plesiosaurs from northern Patagonia. Cretaceous Research 24, 157–170.
Glaessner, M.F., 1980. New Cretaceous and Tertiary crabs (Crustacea: Brachyura) from Australia and New Zealand. Transactions of the Royal Society of South Australia 104, 171–192.
Groβmann, F., 2007. The taxonomic and phylogenetic position of the Plesiosauroidea from the Lower Jurassic *Posidonia* Shale of south-west Germany. Palaeontology 50, 545–564.
Hiller, N., Mannering, A., Jones, C., Cruickshank, A.R.I., 2005. The nature of *Mauisaurus haasti* Hector, 1874 (Reptilia: Plesiosauria). Journal of Vertebrate Paleontology 25, 588–601.
Hiller, N., O'Gorman, J.P., Otero, R.A., 2014. A new elasmosaurid plesiosaur from the lower Maastrichtian of North Canterbury, New Zealand. Cretaceous Research 50, 27–37.
Hiller, N., O'Gorman, J.P., Otero, R.A., Mannering, A.A., 2017. A reappraisal of the Late Cretaceous Weddellian plesiosaur genus *Mauisaurus* Hector, 1874. New Zealand Journal of Geology and Geophysics. http://dx.doi.org/10.1080/00288306.2017.1281317.
Isaac, M.J., Moore, P.R., Joass, Y.J., 1991. Tahora Formation: the basal facies of a Late Cretaceous transgressive sequence, northeastern New Zealand. New Zealand Journal of Geology and Geophysics 34, 227–236.
Keyes, I.W., 1977. Records of the northern hemisphere Cretaceous sawfish genus *Onchopristis* (order Batoidea) from New Zealand. New Zealand Journal of Geology and Geophysics 20, 263–272.
McKee, J.W.A., Wiffen, J., 1998. Mangahouanga Stream- New Zealand's Cretaceous Dinosaur and Marine Reptile Site. 1998 Hector Day Fieldtrip Guide. Geological Society of New Zealand Miscellaneous Publication 96, 18 pp.
Mook, C.C., 1921. Individual and age variations in the skulls of recent Crocodilia. Bulletin of the American Museum of Natural History 54, 51–66.
O'Gorman, J.P., 2016. A small body sized non-aristonectine elasmosaurid (Sauropterygia, Plesiosauria) from the Late Cretaceous of Patagonia, with comments

on the relationships of the Patagonian and Antarctic elasmosaurids. Ameghiniana 53, 245–268.
O'Gorman, J.P., Coria, R., 2016. A new elasmosaurid specimen from the upper Maastrichtian of Antarctica: new evidence of amonophyletic group of Weddellian elasmosaurids. Alcheringa 41, 1–10. http://dx.doi.org/10.1080/03115518.2016.1224318.
O'Gorman, J.P., Gasparini, Z., Salgado, L., 2014. Reappraisal of *Tuarangisaurus? cabazai* (Elasmosauridae, Plesiosauria) from the Upper Maastrichtian of northern Patagonia, Argentina. Cretaceous Research 47, 39–47.
O'Gorman, J.P., Salgado, L., Olivero, E.B., Marenssi, S.A., 2015. *Vegasaurus molyi*, gen. et sp. nov. (Plesiosauria, Elasmosauridae), from the Cape Lamb Member (lower Maastrichtian) of the Snow Hill Island Formation, Vega Island, Antarctica, and remarks on Wedellian Elasmosauridae. Journal of Vertebrate Paleontology 35, e931285.
O'Gorman, J.P., Otero, R.A., Hiller, N., Simes, J., Terezow, M., 2017. Redescription of *Tuarangisaurus keyesi* (Sauropterygia; Elasmosauridae), a key species from the uppermost Cretaceous of the Weddellian Province. Internal skull anatomy and phylogenetic position. Cretaceous Research 71, 118–136.
O'Keefe, F.R., 2004. Preliminary description and phylogenetic position of a new plesiosaur (Reptilia: Sauropterygia) from the Toarcian of Holzmaden, Germany. Journal of Paleontology 78, 973–988.
Otero, R.A., 2016. Taxonomic reassessment of *Hydralmosaurus* as *Styxosaurus*: new insights on the elasmosaurid neck evolution throughout the Cretaceous. PeerJ 4 e1777, 1–60.
Otero, R.A., Soto-Acuña, S., Rubilar-Rogers, D., 2012. A postcranial skeleton of an elasmosaurid plesiosaur from the Maastrichtian of central Chile, with comments on the affinities of Late Cretaceous plesiosauroids from the Weddellian Biogeographic Province. Cretaceous Research 37, 89–99.
Otero, R.A., O'Gorman, J.P., Hiller, N., 2015. Reassessment of the upper Maastrichtian material from Chile referred to *Mauisaurus* Hector, 1874 (Plesiosauroidea: Elasmosauridae) and the taxonomical value of the hemispherical propodial head among austral elasmosaurids. New Zealand Journal of Geology and Geophysics 58, 252–261.
Owen, R., 1860. On the orders of fossil and recent Reptilia and their distribution in time. Report of the British Association for the Advancement of Science 29, 153–166.
Romer, A.S., 1956. Osteology of the Reptiles. Krieger Publishing Company. Florida, Malabar, 792 pp.
Sachs, S., Hornung, J.J., Kear, B.P., 2016. Reappraisal of Europe's most complete Early Cretaceous plesiosaurian: Brancasaurus brancai Wegner, 1914 from the "Wealden facies" of Germany. PeerJ 4 e2813, 79 pp.
Sato, T., Hasegawa, Y., Manabe, M., 2006. A new elasmosaurid plesiosaur from the Upper Cretaceous of Fukushima, Japan. Palaeontology 49, 467–484.
Vajda, V., Raine, J.I., 2010. A palynological investigation of plesiosaur-bearing rocks from the Upper Cretaceous Tahora Formation, Mangahouanga, New Zealand. Alcheringa: An Australasian Journal of Palaeontology 34, 359–374.
Vincent, P., 2010. A juvenile plesiosaur specimen from the Lower Jurassic of Holzmaden, Germany. Palaeontographica Abteilung A 291, 45–61.
Warren, G., Speden, I.G., 1978. The Piripauan and Haumurian stratotypes (Mata Series: Upper Cretaceous) and correlative sequences in the Haumuri Bluff District, South Marlborough. New Zealand Geological Survey Bulletin 92, 1–60.
Wegner, T.H., 1914. *Brancasaurus brancai* n. g. n. sp., ein Elasmosauride aus dem Wealden Westfalens. In: Festschrift für Wilhelm Branca zum 70. Geburtstage 1914. Borntraeger, Leipzig, pp. 235–305.
Welles, S.P., 1949. A new elasmosaur from the Eagle Fort Shale of Texas. Fondren ScienceSeries 1, 1–28.
Welles, S.P., 1952. A review of the North American Cretaceous elasmosaurs, 29. University of California Publications in Geological Sciences, pp. 47–144.
Welles, S.P., 1962. A new species of elasmosaur from the Aptian of Colombia and a review of the Cretaceous plesiosaurs, 44. University of California Publications in Geological Sciences, pp. 1–96.
Werneburg, I.K., Polachowski, M., Hutchinson, M.N., 2015. Bony skull development in the Argus monitor (Squamata, Varanidae, *Varanus panoptes*) with comments on developmental timing and adult anatomy. Zoology 118, 255–280.
Wiffen, J., 1980. *Moanasaurus*, a new genus of marine reptile (Family Mosasauridae) from the Upper Cretaceous of North Island, New Zealand. New Zealand Journal of Geology and Geophysics 23, 507–528.
Wiffen, J., 1981. The first Late Cretaceous turtles from New Zealand. New Zealand Journal of Geology and Geophysics 24, 293–299.
Wiffen, J., 1983. The first record of *Pachyrhizodus caninus* Cope (Order Clupeiformes) from the Late Cretaceous of New Zealand. New Zealand Journal of Geology and Geophysics 26, 109–119.
Wiffen, J., 1990a. *Moanasaurus mangahouangae* or *Mosasaurus mangahouangae*? New Zealand Journal of Geology and Geophysics 33, 87–88.
Wiffen, J., 1990b. New mosasaurs (Reptilia; Family Mosasauridae) from the Upper Cretaceous of North Island, New Zealand. New Zealand Journal of Geology and Geophysics 33, 67–85.
Wiffen, J., McKee, J., 1990. Mangahouanga Stream—Cretaceous vertebrate site. In: Campbell, H.J., Hayward, B.W., Mildenhall, D.C. (Eds.), Geological Society of New Zealand Annual Conference Field Trips, 50b. Geological Society of New Zealand Miscellaneous Publication, pp. 26–30. November 1990, Napier, New Zealand, 189–202.
Wiffen, J., Moisley, W., 1986. Late Cretaceous reptiles (families Elasmosauridae, Pliosauridae) from the Mangahouanga Stream, North Island, New Zealand. New Zealand Journal of Geology and Geophysics 29, 205–252.
Wiffen, J., Molnar, R., 1988. First pterosaur from New Zealand. Alcheringa 12, 53–59.
Young, M.D., Hannah, M.J., 2010. Dinoflagellate biostratigraphy of the vertebrate fossil-bearing Maungataniwha Sandstone, northwest Hawke's Bay, New Zealand. New Zealand Journal of Geology and Geophysics 53, 81–87.